Title: **A Dapl1+ subpopulation of naïve CD8 T cells contains committed precursors of memory lineage.**

Authors: Adam Lynch (first author), Kaito A. Hioki, Xueting Liang, Iris Thesmar, Julia Cernjul, Xinjian He, Jesse Mager, Wei Cui, Dominique Alfandari, Elena L. Pobezinskaya (last author), Leonid A. Pobezinsky (last author).

Key words: stem-like, memory CD8 T cells, differentiation, thymus, let-7, Lin28b, neonatal, T regulatory cells, CD62L, Tim-3

Affiliations + emails

Adam Lynch:

Aclynch@umass.edu

Animal Biotechnology and Biomedical Sciences Program, University of Massachusetts, Amherst, MA, USA

Department of Veterinary and Animal Science, University of Massachusetts, Amherst, MA, USA

UMass Biotech Training Program (BTP), Amherst, MA, USA

Kaito A. Hioki:

Khioki@umass.edu

Molecular and Cellular Biology Program, University of Massachusetts, Amherst MA, USADepartment of Veterinary and Animal Science, University of Massachusetts, Amherst, MA, USA

UMass Biotech Training Program (BTP), Amherst, MA, USA

Xueting Liang:

Xuetingliang@umass.edu

Animal Biotechnology and Biomedical Sciences Program, University of Massachusetts, Amherst, MA, USA
Department of Veterinary and Animal Science, University of Massachusetts, Amherst, MA, USA
Iris Thesmar:
lthesmar@umass.edu
Molecular and Cellular Biology Program, University of Massachusetts, Amherst MA, USA
Department of Veterinary and Animal Science, University of Massachusetts, Amherst, MA, USA
Julia Cernjul:
Jcernjul@umass.edu
Department of Veterinary and Animal Science, University of Massachusetts, Amherst, MA, USA
Xinjian He:
xinjianhe@umass.edu
Animal Biotechnology and Biomedical Sciences Program, University of Massachusetts, Amherst, MA, USA
Department of Veterinary and Animal Science, University of Massachusetts, Amherst, MA, USA
Jesse Mager:
jmager@umass.edu
Department of Veterinary and Animal Science, University of Massachusetts, Amherst, MA, USA
Wei Cui:
wcui@umass.edu
Department of Veterinary and Animal Science, University of Massachusetts, Amherst, MA, USA
Dominique Alfandari:
alfandar@vasci.umass.edu
Department of Veterinary and Animal Science, University of Massachusetts, Amherst, MA, USA
Elena L. Pobezinskaya:
pobeinskaya@umass.edu

Department of Veterinary and Animal Science, University of Massachusetts, Amherst, MA, USA

Leonid A. Pobezinsky:

lpobezinsky@umass.edu

Department of Veterinary and Animal Science, University of Massachusetts, Amherst, MA, USA

ONE-SENTENCE SUMMARY:

Naïve Dapl1 positive CD8 T cells include a pre-programmed subset biased toward differentiation into memory-like T cells.

SUMMARY

Memory CD8 T cells play a vital role in providing lasting immune protection, yet their origins remain incompletely understood. Contrary to classical models, emerging evidence suggests that heterogeneity within the naïve T cell pool may influence fate decisions prior to antigen encounter. However, the markers of naïve T cell heterogeneity have not yet been clearly defined. Here, we describe intraclonal heterogeneity within the naïve T cell population marked by the protein Dapl1. Using novel monoclonal antibodies and a reporter-knockout mouse model, we found that Dapl1-positive naïve CD8 T cells exhibit distinct phenotypes compared to their Dapl1-negative counterparts. Furthermore, this population includes a subset of pre-programmed precursors biased toward memory lineage fate. The differentiation of these precursors is independent of Dapl1 but relies on the transcription factor Bcl11b, resulting in the generation of Dapl1-positive central memory-like CD8 T cells in response to infection, and stem-like memory cells in response to cancer. Notably, naïve Dapl1-positive T cells originate in the thymus among mature thymocytes and gradually appear in the periphery within several days after birth. Our findings suggest that committed memory precursors in the Dapl1-positive population may represent an alternative pathway for memory CD8 T cell generation, offering new avenues for therapeutic application.

INTRODUCTION

CD8 T lymphocytes are indispensable for immune defense, targeting and eliminating host cells infected with intracellular pathogens or transformed by cancer. After antigen clearance, most effector cytotoxic T lymphocytes (CTLs) undergo apoptosis, with only a small fraction persisting as memory CD8 T cells. These memory cells play critical roles in long-term immune protection, rapidly responding to antigen re-exposure, and are central to tumor immunotherapies, including adoptive T cell transfer, CAR-T therapy, and checkpoint blockade [1-16]. Furthermore, memory CD8 T cells are essential for the efficacy of vaccines, making their study important for advancing immunotherapies and vaccine development.

Although much progress has been made, the molecular mechanisms underlying memory CD8 T cell differentiation remain incompletely understood. Two competing models have sought to explain memory T cell ontogeny. The “linear” model suggests that memory cells arise from effector cells, while the “bifurcative” model suggests that asymmetric division of activated CD8 T cells generates distinct effector and memory lineages [17-27]. Despite their differences, both models share the assumption that memory fate is determined during antigen-driven differentiation in the immune response. Recent findings, however, challenge this paradigm, suggesting that heterogeneity within the naïve T cell population may predetermine memory or effector potential before antigen stimulation [28-39]. Progress in this area remains hindered by the absence of reliable markers to identify such heterogeneity, highlighting the need for innovative approaches to unravel the origins of memory CD8 T cells.

Here, we report a new marker Death Associated Protein Like-1 (Dapl1), the expression of which reveals the heterogeneity of naïve T cells. The *Dapl1* gene encodes a 108 amino acids intracellular protein with predicted localization in the cytoplasm. Although very little is known about Dapl1 protein function, it has been reported that Dapl1 may interact with many major pathways including MYC-, MAPK-, NFκb- and NFAT-cascades [40-45]. Furthermore, in other models, Dapl1 is portrayed as a potential “gate keeper” of stem-like phenotypes, suppressing generation of reactive

130 oxygen species and protein translation [46,47]. It has been demonstrated that Dapl1 is highly
131 expressed in skin, retina, and testis. Furthermore, the *Dapl1* gene appeared among the top DEGs
132 in stem-like memory CD4 and CD8 T cells in many recent studies [15,48-63]. The generation of anti-
133 Dapl1 monoclonal antibodies and a Dapl1-reporter mouse model enabled us to detect and study
134 Dapl1-expressing T cells. With these tools, we identified a distinct subpopulation of Dapl1+ cells
135 within naïve T lymphocytes, revealing an additional layer of heterogeneity. Furthermore, we found
136 that within the Dapl1+ CD8 T cells, a subset of pre-programmed lymphocytes preferentially
137 differentiates into memory-like cells during immune responses to pathogens and cancer. Thus,
138 our findings uncover a complementary mechanism contributing to memory formation in CD8 T
139 cells.
140

141 **RESULTS**

142 **<u>1. Dapl1 expression reveals heterogeneity of naïve T cells.</u>**

143 Previously, we demonstrated that the expression of let-7 miRNAs significantly promotes
144 generation of memory CD8 T cells[15]. We found that evolutionary conserved *Dapl1* gene is among
145 the top differentially expressed genes (DEGs) between let-7-transgenic (Let-7Tg) and let-7-
146 deficient (Let-7KD) cytotoxic T lymphocytes (CTLs). Let-7Tg CTLs with memory potential
147 expressed very high levels of *Dapl1* mRNA, while terminally differentiated Let-7KD CTLs had
148 almost none (Fig. 1A).
149 Based on ImmGen RNA-seq data sets [64], we have found that *Dapl1* mRNA expression is restricted
150 to peripheral naive T cells and also persists at lower levels in memory precursors (MPECs) and
151 memory CD8 T cells, but is not present in short lived effector cells (SLECs) (Fig. 1B). Furthermore,
152 recent publications have shown the association of *Dapl1* expression with stem-like memory
153 phenotype for both CD4 and CD8 T cell lineages [15,48-63]. We hypothesized that Dapl1 expression
154 pattern may reflect the gradual loss of multipotent traits of naïve T cells during differentiation into

155 effector cells. Therefore, Dapl1 is a candidate marker for tracing memory lineage cells, where
156 such traits are still preserved.
157 To detect Dapl1-expressing cells, we generated our own monoclonal antibodies (mAbs) against
158 the mouse Dapl1 protein (clone 6H9). The specificity of these anti-Dapl1 mAbs was validated by
159 enzyme-linked immunosorbent assay (ELISA) using recombinant protein and by western blot
160 (WB) with Dapl1-transduced NIH 3T3 cells (fig. S1, A and B). The 6H9 mAbs identified a 12 kDa
161 band corresponding to Dapl1 protein in both CD4 and CD8 T cells from wild-type (WT) mice by
162 WB, but no Dapl1 expression was detected in thymocytes (Fig. 1C), recapitulating the mRNA
163 expression patterns (Fig. 1B). Using the 6H9 mAbs for confocal microscopy, we confirmed the
164 predicted cytoplasmic localization of Dapl1 within the cells (Fig. 1D and fig. S1C). Unexpectedly,
165 we observed that not all CD8 T cells were Dapl1-positive. In fact, intracellular (IC) staining for flow
166 cytometry revealed that 30-50% of naïve peripheral T cells expressed Dapl1 (Fig. 1E). Notably,
167 the intensity of Dapl1 expression and the frequency of Dapl1+ cells were higher in CD8 T cells
168 than in CD4 T cells (Fig. 1F). We also observed that the proportion of Dapl1+ lymphocytes was
169 slightly elevated in blood compared to secondary lymphoid organs such as spleen and lymph
170 nodes. We next compared the phenotype of Dapl1+ and Dapl1- T cells based on the expression
171 of selected surface markers for naïve and activated T cells (fig. S1D). Uniform manifold
172 approximation and projection (UMAP) analysis of multicolor flow cytometry data revealed that
173 Dapl1+ T cells clustered separately from Dapl1- T lymphocytes for both CD4 and CD8 populations
174 (Fig. 1G). Furthermore, the majority of Dapl1+ CD4 and CD8 T cells exhibited quiescent
175 $CD44^{low}CD122^{low}$ phenotypes and had fewer activated $CXCR3^{hi}$ cells compared to their Dapl1-
176 counterparts (Fig. 1H). In addition, gated naïve ($CD44^{low}CD62L^{hi}$) Dapl1+ CD8 T cells contained
177 a high frequency of Ly6C+ cells and expressed elevated levels of CD5, CD44, CD62L, CD127,
178 and CD122 compared to naïve Dapl1- cells (Fig. 1I and fig. S1,E and F). Thus, Dapl1 expression
179 uncovers previously unrecognized heterogeneity within the naïve CD4 and CD8 T lymphocyte
180 populations.

181

182 **2. Dapl1-reporter model uncovers heterogeneity among many T cell subsets.**

183 To investigate the properties of Dapl1+ T cells, we generated a Dapl1-reporter mouse model,
184 Dapl1^{ZsG}, in which the fusion construct of Dapl1, self-cleaving P2A peptide, and fluorescent
185 protein ZsGreen (ZsG) is expressed under the control of the *Dapl1* gene's promoter and all its
186 regulatory elements (Fig. 2A). Overall, the mice appeared phenotypically identical to littermate
187 controls. At steady state, 30-50% of peripheral T cells in Dapl1$^{ZsG/WT}$ mice were ZsG+ (Fig. 2B).
188 Moreover, the intensity of ZsG expression and the frequency of ZsG+ lymphocytes were higher
189 in CD8 T cells than in CD4 T cells. This expression pattern of ZsG correlates well with Dapl1
190 mRNA (Fig. 1B) and protein (Fig. 1E) expression in WT T lymphocytes. Unexpectedly, we
191 discovered that the *Dapl1*^{ZsG} allele does not result in production of Dapl1 protein, despite mRNA
192 expression (Fig. 2C and fig. S2A). It is possible that extra amino acids of the P2A peptide modify
193 the C-terminus of Dapl1 protein leading to its instability. We confirmed this by overexpressing N-
194 and C-terminal HA-tagged Dapl1 constructs (fig. S2B), where only the N-terminal HA-tag was well
195 tolerated. Thus, serendipitously, we created a *Dapl1*^{ZsG} knockout-reporter allele. By leveraging
196 this model, we utilized heterozygous Dapl1$^{ZsG/WT}$ mice as reporters, with ZsG marking Dapl1-
197 expressing cells. In contrast, homozygous Dapl1$^{ZsG/ZsG}$ mice, which lack Dapl1 expression,
198 allowed us to track "Dapl1-wannabe" cells through ZsG expression.

199 In Dapl1$^{ZsG/WT}$ mice, ZsG expression was restricted to T cells (Fig. 2, D and fig. S2C). In secondary
200 lymphoid organs such as the spleen and lymph nodes, 20-30% of CD4 and 40-50% of CD8
201 TCR$\alpha\beta$ T cells were ZsG+. In contrast, a very small proportion of TCR$\gamma\delta$ T cells and virtually no
202 NKT lymphocytes expressed ZsG. Using double reporter Dapl1$^{ZsG/WT}$Foxp3$^{RFP/RFP}$ mice, we found
203 that CD4 Foxp3+ T regulatory cells (Tregs) contained only 2-5% of ZsG+ cells, while a rare
204 population of CD8 Foxp3+ Tregs had approximately 20% ZsG+ cells (Fig. 2, E and F). Notably,
205 the presence of ZsG+ T cells was comparable between splenic and liver T cell subsets but
206 significantly reduced in the small intestine and colon, particularly among CD8 T cell subsets (Fig.

207 2G-H, and fig. S3, A and B, and S4, A-D). Next, we investigated the phenotype of conventional
208 and regulatory ZsG+ T cells from Dapl1$^{ZsG/WT}$Foxp3$^{RFP/RFP}$ mice. As expected, the conventional
209 (Foxp3-) ZsG+ CD4 and ZsG+ CD8 T cells closely phenocopied WT Dapl1+ T cells stained with
210 anti-Dapl1 mAbs (Fig. 1F and 3A-C, fig. S5A-C). The majority of ZsG+ T cells were naïve with
211 significantly elevated levels of CD5, CD44, CD62L, CD127 and CD122. Similar to Dapl1+ cells
212 from WT mice, ZsG+ CD8 T cells were enriched with Ly6C+ cells. Interestingly, ZsG+Foxp3+ CD4
213 Tregs displayed reduced surface expression of CD5 and CD44, an increased proportion of
214 CD62L+ and Ly6C+ cells, and a lower frequency of PD-1+ cells (fig. S5, D and E). This phenotype
215 may indicate that Dapl1+ Tregs have a less activated state, which aligns with previous reports
216 linking this profile to reduced suppressive function [65-67]. Altogether, our results confirmed that ZsG
217 reliably reports Dapl1+ subpopulations of both CD4 and CD8 T cells in Dapl1$^{ZsG/WT}$ mice.
218 To test whether the heterogeneity of Dapl1 expression is due to differences in T cell receptor
219 (TCR)-specificity, we generated two different TCR-transgenic mice (P14 and OT-I) on a
220 Dapl1$^{ZsG/WT}$Rag2KO background. Based on ZsG expression, we found that similar to polyclonal
221 CD8 T cells, approximately 40% of both naïve P14 and OT-I CD8 T cells expressed Dapl1 (Fig.
222 3D) revealing intraclonal heterogeneity of naïve CD8 T cells. Reanalysis of existing scRNA-seq
223 datasets for naïve P14, OT-I, and polyclonal cells confirmed the presence of both Dapl1+ and
224 Dapl1- CD8 T cells at the mRNA level (Fig. 3E). Furthermore, these cells exhibited markedly
225 different transcriptomes, indicating the presence of two distinct populations (Fig. 3E). Notably,
226 naïve Dapl1+ CD8 T cells upregulated a unique set of genes associated with cytokine signaling,
227 interferon signaling, and immunoregulation, while downregulating genes involved in differentiation
228 and apoptosis [68-73] (Fig. 3F). Together, these findings highlight significant heterogeneity of different
229 T cell subsets even within the monoclonal naïve populations.
230
231 **3. Dapl1+ CD8 T cells have biased differentiation towards memory lineage.**

232 Naïve Dapl1+ and Dapl1- CD8 T cells exhibited significant differences in their phenotype and
233 transcriptional profiles. Therefore, we investigated whether Dapl1+ and Dapl1- naïve CD8 T cells
234 are two separate lineages with unique differentiating potentials. First, we tested the persistence
235 of Dapl1 expression in CTLs generated from bulk naïve P14 CD8 T cells. Based on both
236 endogenous expression of Dapl1 protein and our ZsG reporter, we observed that only a small
237 fraction of differentiated cells were Dapl1+ (Fig. 4, A and B, fig. S6A and B). Next, we examined
238 the phenotype of Dapl1+ and Dapl1- CTLs, using the expression of CD62L as a proxy of memory
239 lineage and Tim-3 for terminally differentiated effector cells[15]. Surprisingly, most Dapl1+ CTLs
240 displayed a memory-like (CD62L+Tim3-) phenotype and expressed low levels of effector markers
241 such as PD-1, 2B4 and CD160. In contrast, Dapl1- CTLs showed significantly higher expression
242 of these molecules and also included a population of terminally differentiated (CD62L-Tim3+)
243 cells. Furthermore, we found that the frequency of ZsG+(Dapl1+) CTLs increased after treatment
244 with rapamycin, a potent inhibitor of TORC1 known to promote the formation of memory cells [74]
245 (Fig. 4C). These results indicate that Dapl1 expression in differentiating cells may be associated
246 with memory formation.
247 The small number of Dapl1+ CTLs may indicate that many cells downregulated Dapl1 expression
248 during the differentiation process. To test this, we generated CTLs *in vitro* from sorted
249 ZsG+(Dapl1+) and ZsG-(Dapl1-) naïve CD8 T cells from P14+Dapl1$^{ZsG/WT}$Rag2-/- mice. Indeed,
250 many initially Dapl1+ cells lost the expression of Dapl1 (Ex-Dapl1) during CTL differentiation and
251 were phenotypically indistinguishable from CTLs derived from naive ZsG-(Dapl1-) cells. In
252 contrast, the small proportion of CTLs that retained ZsG expression had exclusively memory-like
253 phenotypes (CD62L+Tim3-) with reduced levels of effector markers (fig. S6C). Of note, the vast
254 majority of effector descendants of naïve ZsG-(Dapl1-) T cells remained Dapl1-, suggesting
255 limited plasticity from Dapl1- to Dapl1+ subpopulations during differentiation.
256 To directly investigate the fate of differentiating Dapl1+ and Dapl1- CD8 T cells, we employed an
257 *in vivo* infection mouse model, where we used *Listeria monocytogenes* that expressed GP33

258 peptide (LM-GP33), a cognate antigen for P14 TCR-transgenic CD8 T cells. Sorted Dapl1+ and
259 Dapl1- naïve P14 T cells were separately injected into LM-infected host mice and their phenotypes
260 were assayed over time (Fig. 4D). During the immune response, many initially Dapl1+ cells lost
261 Dapl1 expression, becoming Ex-Dapl1 cells, which confirmed our *in vitro* observations.
262 Importantly, the frequency of Dapl1+ cells gradually recovered, with the majority of long-lived
263 memory cells expressing Dapl1. On day 7 and 14 post-infection, CD8 T cells that retained Dapl1
264 expression (ZsG+) had acquired an MPEC phenotype (KLRG1-CD127+), while Ex-Dapl1 cells
265 differentiated into both MPECs and SLECs (KLRG1^{+}CD127^{-}) (Fig. 4E). After 30 days post-
266 infection, most of the Dapl1+ memory cells exhibited the phenotype of central memory CD8 T
267 cells (T_{CM}, CD44^{hi}CD62L+). Overall, the number of generated memory cells was comparable
268 between descendants of Dapl1+ and Dapl1- naïve T cells (fig. S6D). Of note, the differentiated
269 progeny of Dapl1- naïve CD8 T cells remained preferentially ZsG-(Dapl1-) at all times and gave
270 rise to both SLECs and MPECs as expected. In this case, the appearance of a very small
271 proportion of Dapl1+ memory cells (2-4%) can be explained by initial sort impurity or very limited
272 expression of Dapl1 *de novo*. We also noticed that in both *in vitro* and *in vivo* experiments, cells
273 which retained expression of Dapl1 expressed higher surface levels of CD62L than their Dapl1-
274 counterparts (fig. S6C and E), suggesting that Dapl1+ and Dapl1- memory lineage cells may be
275 different. To this end, we reanalyzed publicly available scRNA-seq datasets for P14 T_{CM}, effector
276 memory (T_{EM}) and resident memory (T_{RM}) cells generated in response to acute Lymphocytic
277 Choriomeningitis Virus Armstrong (LCMV-Arm) infection [62,68,70,71,75,76]. We confirmed that a
278 proportion of Dapl1+ cells is present in T_{CM} but not T_{EM} or T_{RM} populations after acute LCMV-Arm
279 infection [68] (fig. S6F). Furthermore, the upregulated DEGs in Dapl1+ T_{CM} cells included genes
280 associated with stem-like memory cell differentiation (*Tcf7, Sox4, Id3, Sell, Slamf6 and etc.*), as
281 well as genes involved in the regulation of translation and survival (Fig 4F, fig. S6G). Conversely,
282 these cells showed a depletion in the expression of genes linked to leukocyte activation. These
283 data demonstrate that differentiated Dapl1+ T cells are transcriptionally different from Dapl1-

284 counterparts and express higher levels of key memory related genes. Overall, these results
285 suggest that the pool of Dapl1+ naïve CD8 T cells harbors a distinct subpopulation pre-committed
286 to memory lineage, with their progeny marked by persistent expression of Dapl1 and unique
287 transcriptional profile. This finding indicates that, for a subset of naïve CD8 T cells, memory fate
288 may be pre-determined prior to antigen encounter (fig. S7A).
289 To define the mechanisms regulating Dapl1+ CD8 T cell differentiation, we focused on the
290 transcription factors (TFs) that were upregulated in Let-7Tg CTLs where Dapl1 was also strongly
291 expressed [15]. Specifically, we tested the ability of selected TFs (Lef1, Id3, Bach2, Bcl11b, Sox4,
292 Tcf1, Foxo1 and Hif1a) from memory signature genes of Let-7Tg CTLs, to support the
293 differentiation of Dapl1+ CTLs *in vitro*. Compared to the empty-retrovirus (RV) control, WT CTLs
294 transduced with RVs encoding *Bcl11b*, *Klf2*, and *Tcf7* showed robust generation of Dapl1+ CTLs
295 (Fig. 4G, fig. S8A). In addition to Dapl1 expression, these transduced CTLs also exhibited
296 increased frequency of CD62L+ cells and decreased frequency of Tim3+ cells (Fig. 4G, fig. S8A).
297 In contrast, CTLs transduced with TFs involved in effector cell differentiation failed to generate
298 Dapl1+ cells. Given the fact that Bcl11b was the most potent inducer of Dapl1+ CTLs *in vitro* and
299 has been previously implicated in the formation of MPECs and CD8 T memory cells [77,78], we next
300 assessed the expression of Dapl1 in wild-type (WT) and Bcl11b-/- MPECs generated in response
301 LM-OVA infection using publicly available RNA-seq dataset [78]. On day 9 post infection (dpi), in
302 addition to compromised cell numbers [78], Bcl11b-/- MPECs had significantly reduced expression
303 of Dapl1 mRNA compared to WT cells (fig. S8B), while as expected, all SLECs had low Dapl1
304 expression. Altogether, these results suggest that the transcription factor Bcl11b promotes the
305 differentiation of Dapl1+ memory lineage CD8 T cells.
306 During chronic infection or cancer, effector cells become exhausted (T_{EX}) and the formation of
307 memory cells is altered leading to the generation of a distinct memory lineage known as
308 progenitors of exhausted cells (T_{PEX}) with stem-like potential [3,6-8,16]. Importantly, these stem-like
309 cells are the primary responders to various tumor treatments including immunotherapies such as

310 T cell adoptive transfer, CAR-T, and checkpoint blockade. Phenotypically, T_{PEX} express CD62L,
311 Ly108 and low levels of inhibitory receptors like Tim-3 on their surface [3]. We therefore investigated
312 the presence and phenotype of differentiated Dapl1+ T cells within the tumor microenvironment
313 using B16 melanoma mouse model. Approximately 10-20% of Dapl1+ T cells were observed
314 among CD8 tumor infiltrating lymphocytes (TILs) isolated from Dapl1$^{ZsG/WT}$ or WT B16-bearing
315 mice (stained with 6H9 mAbs). These cells were antigen experienced (CD44^{hi}) and displayed the
316 T_{PEX} phenotype (CD62L+Tim-3- and Ly108^{hi}) (fig. S9, A-C). The reanalysis of available TILs
317 scRNA-seq dataset further confirmed our findings that T_{PEX} but not terminally differentiated T_{EX}
318 cells contain a Dapl1+ population [50] (fig. S9E). Furthermore, the upregulated DEGs in Dapl1+
319 CD8 TILs included genes shared with Dapl1+ T_{CM} cells and are linked to a stem-like memory cell
320 profile (*Tcf7, Sox4, Id3, Sell, Slamf6 and etc.*), cell differentiation, translation and survival [6,11,50,79-
321 81] (fig. S9F and G). These data suggest that during anti-tumor immune responses, a pre-
322 committed subpopulation of naïve Dapl1+ cells also exhibits differentiation bias and contributes
323 to the formation of stem-like memory CD8 T cells in TILs.
324

325 **4. Dapl1 expression is required for maintenance of Dapl1+ memory CD8 T cells but not for**
326 **their differentiation.**

327 The role of Dapl1 in differentiation of memory CD8 T cells is unknown. To explore this question,
328 we took advantage of our mouse model, where homozygosity of the Dapl1-reporter allele results
329 in Dapl1 deficiency (Fig. 2C). In Dapl1$^{ZsG/ZsG}$ mice, ZsG expression serves as a marker for Dapl1-
330 deficient T cells, allowing us to track and characterize these “wannabe” cells. After adoptive
331 transfer of naïve Dapl1$^{WT/WT}$ or Dapl1$^{ZsG/ZsG}$ P14 T cells followed by LM-GP33 infection, we
332 consistently observed a mild but significant decrease in the proportion of Dapl1-wannabe cells at
333 every stage of the immune response including formation of memory cells (Fig. 5A), while the
334 phenotype of Dapl1-wannabes resembled the memory lineage phenotype of Dapl1+ cells (Fig.
335 5B, Fig. S10A). We obtained similar results in differentiation experiments *in vitro* (fig. S10B). Of

336 note, loss of Dapl1 expression had no impact on the generation of Dapl1-wannabe TILs or their
337 stem-like memory phenotype in Dapl1$^{ZsG/ZsG}$ mice (fig. S10C). Furthermore, in a separate *in vivo*
338 experiment the phenotype of differentiating CD8 T cells transduced with Dapl1-RV was
339 indistinguishable from that of cells transduced with an empty-RV control, indicating that Dapl1
340 overexpression does not affect the lineage fate of CD8 T cells (fig. S10D). Thus, our results
341 suggest that Dapl1 may play a positive role in maintenance of differentiating cells rather than the
342 control of their fate.
343 We next sought to test functional differences between Dapl1+ and Dapl1 wannabe memory CD8
344 T cells. Restimulation of memory cells collected 30+ days post infection demonstrated that true
345 Dapl1 positive memory CD8 T cells contained a higher proportion of polyfunctional (Ifnγ+Tnfα+)
346 cells compared to Dapl1-wannabe or Dapl1- memory T cells (Fig. 5C). However, adoptively
347 transferred sorted P14 Dapl1$^{WT/WT}$ and Dapl1$^{ZsG/ZsG}$ memory T cells control B16-GP33 tumor
348 growth with similar efficiency in tumor-bearing mice suggesting that the absence of Dapl1 does
349 not affect the overall performance of memory T cells (fig. S10E). Additionally, although a previous
350 report suggests that mice with a global CRISPR-mediated knockout of Dapl1 exhibit enhanced
351 effector function of CD8 T cells in anti-tumor immune responses [45], we did not observe differences
352 in MC38 tumor growth control between Dapl1$^{ZsG/ZsG}$ and Dapl1$^{WT/WT}$ mice, pointing to potential
353 discrepancies between these two models of Dapl1-deficiency (fig. S10F). Collectively, our findings
354 suggest that while Dapl1 is dispensable for the generation and function of memory CD8 T cells,
355 it contributes to the maintenance of memory lineage cells and production of effector cytokines.
356

357 **5. The development of naïve Dapl1+ T cells.**

358 Previous studies have shown that neonatal CD8 T cells exhibit reduced memory potential and
359 tend to differentiate into SLECs rather than MPECs or memory cells [34,82,83]. Based on this, we
360 hypothesized that the development of Dapl1+ T cells may be limited in neonatal mice. To test this,
361 we assessed the frequency of naïve Dapl1+ T cells in the spleens of Dapl1$^{ZsG/WT}$ mice at day 1,

362 one week, and one month after birth. In one-day-old neonatal mice, no Dapl1+ T cells were
363 detected in the periphery. However, these cells gradually appeared with age (Fig. 6A), suggesting
364 a developmental delay in generating Dapl1+ T cells during the neonatal period.
365 We then examined whether Dapl1+ T lymphocytes originate within the thymus before populating
366 secondary lymphoid organs or if they arise directly in peripheral tissues. In the adult thymus, we
367 detected a small population of Dapl1+ cells only among mature CD4 and CD8 single positive (SP)
368 thymocytes (Fig. 6B, fig. S11A). To confirm these findings, we analyzed Dapl1 mRNA levels in
369 bulk RNA-seq dataset of sorted thymocyte populations at different developmental stages [84]. The
370 results corroborated that only post-selected thymocytes expressed Dapl1 (Fig. 6C). Additionally,
371 projecting Dapl1 expression on pseudotime analysis of thymocyte scRNA-seq dataset indicated
372 that Dapl1 mRNA expression is indeed upregulated in a subset of the most mature thymocytes [85]
373 (Fig. 6D).
374 To investigate whether the mature Dapl1+ T cells found in the thymus could originate from
375 recirculation from the periphery, we utilized CD24 as a marker of thymocyte maturation. The
376 surface expression of CD24 is highest on immature thymocytes and declines with maturation,
377 while peripheral T cells are generally CD24-negative. We observed that ZsG+(Dapl1+)TCR+ CD8
378 thymocytes exhibited intermediate levels of CD24 – lower than immature double-positive
379 thymocytes but significantly higher than peripheral T cells from lymph nodes (Fig. 6E) suggesting
380 their thymic origin. Moreover, the lower CD24 expression on ZsG+(Dapl1+)TCR+ CD8
381 thymocytes compared to mature ZsG-(Dapl1-)TCR+ CD8 thymocytes indicated that Dapl1+ cells
382 represent a more advanced maturation stage. Lastly, ZsG intensity was lower in Dapl1+
383 thymocytes than peripheral T cells (Fig. 6F), altogether ruling out recirculation from the periphery
384 as a likely source.
385 The presence of Dapl1+ T cells among the most mature thymocytes implies that single-positive
386 thymocytes upregulate Dapl1 immediately before exiting the thymus, potentially explaining the
387 low frequency of Dapl1+ cells in thymus relative to peripheral lymphoid organs. To test this, we

388 blocked the T cell egress from the thymus using FTY720, a potent agonist of S1PR1 receptor that
389 is involved in T cell migration [86]. After one week of FTY720 treatment, we observed a significant
390 increase in the proportion of ZsG+(Dapl1+) T cells among mature SP4 and SP8 populations in
391 Dapl1$^{ZsG/WT}$ mice (Fig. 6G), while peripheral ZsG+(Dapl1+) T cell frequency remained unchanged
392 (fig. S11B). Together, these findings demonstrate that Dapl1+ T cells first emerged in the thymus
393 among mature thymocytes shortly before their exit into peripheral lymphoid organs, highlighting
394 the thymus's potential role in pre-programming naïve T cell populations.
395

396 **Discussion**

397 Understanding the origins of memory T cells has been a key focus in immunology. It is generally
398 accepted that the steps leading to memory lineage commitment occur after antigen recognition.
399 Consequently, naïve T cells have been regarded as precursors capable of differentiation into
400 memory and effector cells during immune responses. This bipotential ability was elegantly
401 demonstrated in adoptive transfer experiments of single naïve CD8 T cells [19,21,26]. These and many
402 other fundings support the most popular model of memory formation proposed by Steven Reiner's
403 group, where naïve T cells undergo asymmetric division after antigen encounter, producing one
404 daughter cell committed for the effector lineage and another for the memory lineage [20,22,27]. Here,
405 we report a discovery of a novel subpopulation of naïve CD8 T cells whose differentiation does
406 not align with the conventional model of memory formation. These naïve cells are already pre-
407 committed to differentiate into memory-like lineage cells even before encountering an antigen.
408 They can be identified by persistent expression of the *Dapl1* gene during differentiation, both *in*
409 *vitro* and *in vivo*.

410 Using in-house monoclonal antibodies (6H9) against the Dapl1 protein and a Dapl1-reporter
411 mouse model, we uncovered significant heterogeneity among naïve T cells based on Dapl1
412 expression. At steady state, most of Dapl1+ T cells had a true naïve phenotype and were largely
413 excluded from activated or differentiated subsets. However, they also exhibited distinct features,

414 including slightly elevated levels of CD5, CD44, CD62L, CD122 and CD127 (in CD8 T cells),
415 upregulated expression and frequency of Ly6C, and reduced CD103. This heterogeneity was also
416 observed in naïve CD8 T cells from MHC class I restricted TCR-transgenic mice, indicating
417 previously unrecognized intraconal diversity. Furthermore, scRNA-seq analysis of multiple data
418 sets of naïve CD8 T cells revealed a unique transcriptional signature of Dapl1+ lymphocytes,
419 further supporting their distinct identity within the naïve T cell pool.
420 Intriguingly, during the immune response, a small subset of naïve Dapl1+ CD8 T cells retained
421 Dapl1 expression and differentiated into central memory T cells, while the majority downregulated
422 Dapl1 and showed no apparent fate bias. Notably, naïve Dapl1- cells neither upregulated Dapl1
423 nor exhibited any bias in their differentiation. These findings strongly suggest that within the
424 Dapl1+ naïve CD8 T cell population, a small population (10-20%) is pre-committed to the memory
425 lineage even before antigen stimulation. This previously unrecognized pathway of memory
426 formation adds more complexity to the current model of CD8 T cell differentiation, which is based
427 on the fact that memory lineage commitment occurs only after antigen exposure [17]. Although the
428 pre-programming of naïve CD8 T cells into memory has not been previously described, the
429 hegemony of the bifurcative model has been challenged by a few other findings. For instance,
430 nuclear envelope invaginations have been shown to distinguish naïve CD8 T cells predisposed to
431 differentiate into effector-like cells [30]. Similarly, type-I IFN exposure in naïve CD4 T cells caused
432 a bias toward central memory cell differentiation by influencing their transcriptional and functional
433 programming [28]. Additionally, biased differentiation has been observed between naïve CD5high
434 and CD5low CD4 T cells [33].
435 We found that Dapl1 expression in differentiated cells is associated with the CD8 T cell subsets
436 possessing memory potential, including memory precursors, central memory cells and stem-like
437 cells. This observation aligns with prior studies in which Dapl1 was identified among top DEGs in
438 memory-like lymphocytes [15,48-63]. Furthermore, the transcriptional difference between Dapl1+ and
439 Dapl1- memory cells revealed a new layer of heterogeneity. This raises the possibility that

440 differentiated Dapl1+ lymphocytes represent a novel lineage of memory CD8 T cells. Further
441 research is needed to determine whether these phenotypic differences translate into functional
442 variations and to identify additional markers that can reliably pinpoint memory precursors within
443 the Dapl1+ naïve T cell population.

444 The general biological function of the Dapl1 protein remains largely unexplored. In lower
445 vertebrates such as zebrafish and *Xenopus*, the homologous Dap1b protein functions as a
446 translational inhibitor by directly interacting with ribosomes, rendering them dormant and
447 contributing to ribosomal storage and translational repression [46]. In mammals, Dapl1 has been
448 primarily studied outside the immune system [40-44,47], though one study implicated it in the negative
449 regulation of anti-tumor activity of CD8 T cells [45]. Using our homozygous reporter mouse model,
450 we investigated Dapl1-deficient lymphocytes but did not observe enhanced anti-tumor activity.
451 Instead, we found that Dapl1 expression influences the frequency of Dapl1+ memory CD8 T cells
452 and their production of effector cytokines such as IFNγ and TNFα. Further research is required to
453 elucidate the molecular mechanisms through which Dapl1 drives these observed phenotypes.

454 Among the transcription factors known to promote memory formation, Bcl11b emerged as the
455 most potent in supporting the differentiation of Dapl1+ memory lineage cells *in vitro* and *in vivo*.
456 This aligns with previous studies showing that, beyond its essential role in T cell lineage
457 specification, Bcl11b is required for memory CD8 T cell differentiation and counteracts the innate-
458 effector program [77,78,87]. However, the precise role of Bcl11b in this process remains unclear,
459 including whether it directly regulates Dapl1 expression. Given the critical role of Bcl11b in T cell
460 development, future investigation should determine whether its expression is necessary for the
461 formation of naïve Dapl1+ T cells and whether it contributes to pre-programming of memory
462 precursors within this population.

463 Although most Dapl1+ naïve T cells are located in the periphery, our findings demonstrate that
464 the earliest Dapl1+ naïve T cells can be detected among the most mature thymocytes, suggesting
465 a thymic developmental origin. However, the signals driving the development of Dapl1+ cells in

466 the thymus remained unidentified. It is also unclear whether the memory commitment observed
467 in a subset of Dapl1+ naïve T cells occurs in the thymus or in the periphery. Addressing these
468 questions is of significant interest, as it could inform strategies to enhance vaccine efficiency and
469 improve T cell-based therapies.
470 Furthermore, we found that the development of Dapl1+ T cells is age-dependent. Peripheral
471 Dapl1+ T cells emerge gradually within the first week after birth, coinciding with the transition of
472 the neonatal immune system to an adult-like state. This transition is thought to be governed by a
473 postnatal switch in the source of hematopoietic stem cells (HCSs): from embryonic HSCs derived
474 from liver to adult HSCs originated in the bone marrow [88]. Notably, neonatal CD8 T cells are
475 reported to have diminished memory potential, favoring differentiation into short-lived effector
476 cells [34,82,83]. This process is largely mediated by the transient expression of Lin28b, an RNA-
477 binding protein that inhibits the biogenesis of evolutionary conserved let-7 miRNAs [89,90]. Although
478 Lin28b-transgenic CTLs lack detectable *Dapl1* mRNA expression (Fig. 1A), it remains to be
479 determined whether Dapl1 expression is regulated by let-7.
480 In summary, our study predicts the existence of a novel subpopulation within a pool of Dapl1+
481 naïve CD8 T cells that appears pre-committed to differentiate into memory-like cells even before
482 antigen exposure. Moreover, we demonstrated that Dapl1 expression serves as a valuable marker
483 for tracking the progeny of this population among long-lived cells generated during immune
484 responses to cancer or infection. Future investigations are needed to elucidate the precise roles
485 these cells play in immunity and to uncover the molecular mechanisms underpinning their
486 commitment to memory lineage.
487
488
489
490
491

492 **Materials and methods**

493 Ethics statement

494 This study was performed in accordance with the recommendations in the Guide for the Care and
495 Use of Laboratory Animals of the National Institutes of Health. All animals were handled according
496 to approved institutional animal care and use committee (IACUC) protocols of the University of
497 Massachusetts, Amherst.

498 Animals

499 B6 (C57BL/6J, stock # 000664), *Rag2*$^{-/-}$ (B6.Cg-*Rag2*$^{tm1.1Cgn}$/J, stock # 008449), OT-I (C57BL/6-
500 Tg(TcraTcrb)1100Mjb/J), stock # 003831) and FoxP3^{RFP} (C57BL/6-*Foxp3*^{tm1Flv}/J, stock #
501 008374) mice were obtained from the Jackson Laboratory. P14 (B6;D2-
502 Tg(TcrLCMV)327Sdz/JDvs/J) mice were a generous gift from Alfred Singer (NCI, NIH). Dapl1^{ZsG}
503 mice were generated in the University of Massachusetts Animal Models core facility (see below).
504 P14^{+}Lin28Tg and P14^{+}let-7Tg mice on a *Rag2*$^{-/-}$ background were generated as previously
505 described [91]. Animals were housed in a specific pathogen-free facility under a 12-h dark/12-h light
506 cycle at 20–22 °C and a humidity range of 30–70%. All breedings were maintained at the
507 University of Massachusetts, Amherst.

508 Generation of Dapl1^{ZsG} mice

509 Dapl1^{ZsG} knock-in mice were generated in the University of Massachusetts Animal Models core
510 facility using CRISPR/Cas9-mediated genome editing. The knock-in template construct was
511 designed to replace the Stop codon of the *Dapl1* gene and contained a GSG-P2A-ZsGreen
512 fragment flanked by 120bp 5' and 3' homology arms. Two single guide RNAs (sgRNA) were used
513 to target PAM (AGG) 10 bp upstream (antisense sgRNA1: GTCCTGGTCTAACATTTTCG) and
514 PAM (AGG) 3 bp downstream (sense sgRNA2: AACCTCGAAAATGTTAGACC) of Stop codon of
515 the *Dapl1* gene, such that the original target sequence is disrupted after insertion of the construct
516 and therefore is no longer subject to Cas9 re-cutting. Single-strand DNA template (GenScript,
517 Inc), Cas9 protein, and sgRNAs (IDT, Inc) were microinjected into zygotes isolated from

518 superovulated B6D2F1 (C57BL/6J × DBA2J) female mice (8–10 weeks old) mated with B6D2F1
519 males, followed by euthanasia 20 h post-hCG injection for zygote collection from the oviducts.
520 Microinjected zygotes were cultured in KSOM medium (EMD Millipore) at 37°C in a humidified
521 atmosphere of 5% CO_2/5% O_2 balanced with N_2. After 3 days of in vitro culture, early blastocysts
522 (E3.5) were transferred into the recipients (E2.5) by using Nonsurgical Embryo Transfer
523 (ParaTechs Corporation, #60010) to produce founder mice. Correctly targeted mice (identified by
524 PCR using the primers for 5' end Dapl1F GTAGAGACTGCGACTTGACC/ZsGreenR
525 CTTCATGGTCATCTCCTTGG and for 3' end ZsGreenF TCCTGCGAGAAGATCATCC/Dapl1R
526 GAAAAGGGAAGATACAAAAGTTGG, and confirmed by sequencing) were backcrossed to
527 C57BL/6J mice for 10 generations.

528 Generation of anti-Dapl1 antibodies

529 Anti-Dapl1 antibodies were generated as described previously [92]. Briefly, recombinant Dapl1
530 protein was cloned and expressed using Novagen pET Expression System (EMD Millipore)
531 according to manufacturer's instructions. 8-week-old BalbC/J mice were immunized
532 intraperitoneally with 100 µg of the purified Dapl1 protein mixed in with Freund adjuvant. Spleens
533 were harvested after two boosts and splenocytes were fused with SP20 myeloma cells (ATCC)
534 using electrofusion (BTX, Harward apparatus). Hyrbidomas were cultured in RPMI supplemented
535 with 20% fetal bovine serum, 100 U/mL penicillin, 0.1 mg/mL streptomycin, 2 mM L-glutamine, 1
536 mM sodium pyruvate and HAT (0.1 mM sodium hypoxanthine, 0.4 µM aminopterin, 16 µM
537 thymidine). Hybridomas were tested by ELISA on the Dapl1 protein and immunofluorescence on
538 NIH-3T3 cells transfected with Dapl1.

539 Flow cytometry analysis

540 Flow cytometry data were acquired on BD LSR Fortessa or Cytek™ AURORA and analyzed in
541 FlowJo™ v10.9.0 Software. The following monoclonal antibodies from BioLegend were used:
542 CD8α (53-6.7), CD8β (YTS156.7.7), CD4 (RM4-5), CD44 (IM7), CD62L (MEL-14), KLRG1
543 (2F1/KLRG1), CD127 (A7R34), PD1 (29F.1A12), Tim-3 (RMT3-23), 2B4 (m2B4(B6)458.1),

544 CD45.2 (104), CD122 (TM-β1), CD5 (53-7.3), TCRβ (H57-597), TCRγ/δ (GL3), CD11b (M1/70),
545 Ly6c (HK1.4), Ly6g (1A8), CD3 (145-2C11), NK1.1 (PK136), B220 (RA3-6B2), F480 (BM8),
546 SiglecH (551), CD11c (N418), CD24 (M1/69), CD172 (P84), CXCR3 (CXCR3-173), CD103 (2E7),
547 Ly108 (330-AJ), TNFα (MP6-XT22) and Streptavidin - AF647, PE, BV711. CD160 (CNX46-3),
548 MHCII (M5/114.15.2) and IFNγ (XMG 1.2) were from eBioscience. CD45 (30-F11) was from
549 Invitrogen. PE-CF594 rat anti-mouse IgG was from BD Biosciences. PE-conjugated CD1d
550 tetramers were obtained from the Tetramer Core Facility of the US National Institutes of Health.
551 Live cells were incubated with anti-CD16/32 Fc block (2.4G2, BD Pharmingen) prior to staining
552 with antibodies against surface markers. Staining for surface proteins was performed at 4 °C for
553 40 min, and FACS buffer (PBS + 0.5% BSA + 0.01% sodium azide) was used for washes. Dead
554 cells were stained with DAPI.
555 For intracellular cytokine staining, cell suspensions were restimulated *in vitro* for a total of 4 hours
556 with 50 ng/mL phorbol 12-myristate 13-acetate (PMA, Sigma) and 1 μM Ionomycin (Sigma), in
557 the presence of 2 μM monensin (eBioscience). After surface antibody staining, cells were stained
558 with the LIVE/DEAD fixable Blue Dead Cell Stain Kit (Thermo Fisher Scientific) according to the
559 manufacturer's instructions. Cells were then fixed and permeabilized using the Cytofix/Cytoperm
560 solution kit (BD Biosciences) according to the manufacturer's instructions, followed by staining
561 with antibodies against intracellular molecules, including Dapl1.
562 Data from Cytek™ AURORA were gated on live CD45+ TCRβ+ cells (fig. 1G, 3A) or total live
563 CD45+ cells (fig. 2E) and exported to csv files as channel values with all compensated
564 parameters. The exported data were analyzed by the Seurat package [93] using R software version
565 4.2.1. Data were loaded as count matrices and converted to a Seurat object using the
566 CreateSeuratObject() function. Fluorescence intensity representing DAPL1 expression was
567 added to the metadata and included (fig. 1G, 3A) or excluded (fig. 2E) as a variable for clustering.
568 Data were normalized, scaled, and all features were used for PCA and UMAP analyses. Clusters

569 were annotated based on the fluorescence level of cell type markers. Cells representing CD4+ or
570 CD8+ cells were subset and re-clustered (fig. 1G, 3A).

571 Cell isolation

572 Lymph nodes, spleens and thymuses were gently tweezed to isolate lymphocytes. ACK lysing
573 buffer (KD Medical) was used to remove red blood cells from spleen suspensions. For purification
574 of CD8 or CD4 T cells, lymphocyte suspensions were incubated with anti-mouse CD4 (GK1.5) or
575 anti-mouse CD8 (2.43) antibodies, respectively, followed by incubation with anti-rat IgG magnetic
576 beads (BioMag, Qiagen).

577 For the isolation of IELs and LPLs, the small intestine and colon were first removed from the rest
578 of the gastrointestinal tract, onto collection media (RPMI supplemented with 25mM HEPES, 1%
579 L-glutamine, 1% penicillin/streptomycin, 50μM β-mercaptoethanol, and 3% FBS). Peyer's
580 patches lining the small intestine were removed. Tissues were cleaned by flushing out feces with
581 collection media and rinsing in PBS. Tissue fragments were agitated at 37°C for 20 minutes in
582 collection media containing 5mM EDTA and 1mM DTT, then further shaken in serum-free
583 collection media containing 2mM EDTA. The suspension was washed several times in collection
584 media and passed through a 70μm filter. For LPLs, tissue fragments were minced and agitated at
585 37°C for 25 minutes in serum-free collection media containing 1mg/mL Collagenase D and
586 0.5mg/mL DNAse. The suspension was passed through a 70μm filter, washed in collection media,
587 then purified by a 30% Percoll gradient. Finally, IELs and LPLs were resuspended in collection
588 media containing 10% FBS.

589 For TIL isolation, mice were injected subcutaneously in the right flank with 2.5 x 10^5 tumor cells.
590 On day 8, mice were intravenously injected with CD45.2-BV785 antibodies (3 mg per mouse).
591 Tumors were collected 3 minutes post-injection. They were then minced and passed through a
592 40-micron filter, spun at 1250 rpm for 5 min, and resuspended in FACS buffer.

593 For isolation of liver lymphocytes, livers of mice were perfused with 10mL PBS, followed by
594 collection and manual disassociation of tissues via filtration through a 40-micron filter. Cells were

595 then spun at 1250 rpm for 5 minutes, followed by resuspension in 5mL 37% Percoll at room
596 temperature. Resuspended cells were separated by a 20-minute room temperature spin at 800G.
597 The uppermost layers of fluid were carefully aspirated to preserve the lymphocyte pellet, which
598 was then stained for flow cytometry.

599 *In vitro* culture

600 All cultures were kept in 37°C and 7% CO_2 atmosphere in a humidified incubator. For CTL
601 generation, CD8 T cells were stimulated with irradiated splenocytes and soluble anti-CD3 mAbs
602 (1 µg/mL). Cells were cultured in RPMI supplemented with 10% fetal bovine serum, 1% HEPES,
603 1% sodium pyruvate, 1% penicillin/ streptomycin, 1% L-glutamine, 1% non-essential amino acids
604 and 0.3% β-mercaptoethanol. 48h after activation, IL-2 was added to culture media (100 U/mL)
605 and cells were differentiated for an additional 3 days. For CTL differentiation with inhibitors,
606 rapamycin (Sigma-Aldrich) was used at the final concentration of 0.5µM for the first 48 hours of
607 culture. For 24-hour activations, T cells were stimulated with plate-bound anti-CD3 mAbs (1
608 µg/mL) and anti-CD28 mAbs (5 µg/mL).

609 NIH-3T3, MC38 and Jurkat cells were obtained from ATCC. B16-GP33 [15] and NIH-3T3 cells were
610 cultured in DMEM supplemented with 10% FBS. Jurkat and MC38 cells were cultured in RPMI
611 supplemented with 10% FBS.

612 *In vivo* tumor experiments

613 After receiving a sublethal dose of irradiation (500 Rad), mice were injected subcutaneously in
614 the right flank with 2.5 x 10^5 MC38 cells. For studies involving adoptive T cell transfer, irradiated
615 mice were injected intravenously with 5 x 10^4 P14+ memory cells [94], followed by subcutaneous
616 injection of 2.5 x 10^5 B16-GP33 cells the next day. Tumors were measured every 2-3 days with a
617 caliper and tumor volume was determined using the following formula: ½ x D x d^2 where D is the
618 length and d is the width. Mice were euthanized when tumors reached 2 cm^3, when tumors
619 became ulcerated, or in instances when tumors interfered with normal behavior.

620 Confocal Microscopy

621 For microscopy, iBiTreat dishes (u-slide 8 well, 80826-90) were coated with 5μg/mL fibronectin
622 overnight, then washed before seeding $1x10^4$ NIH-3T3 cells per cell. NIH-3T3 cells were imaged
623 one day after seeding the iBiTreat dishes. Cultures were rinsed with PBS, then fixed with 3.7%
624 formaldehyde at room temperature for 25 minutes. After rinsing three times with PBS, cells were
625 permeabilized with 0.5% Triton at room temperature for 5 minutes. Cells were blocked with PBS
626 containing 1% BSA for 1 hour at room temperature. Cells were stained as described in "Flow
627 cytometry analysis", using PBS + 1% BSA for washes. For naïve P14 T cells, cells in suspension
628 were stained, fixed, and permeabilized as described above. Stained cells were mixed with
629 ProLong Gold (Thermo Fisher Scientific, P36934), and sealed onto a glass slide with a coverslip.
630 Images were taken with a Nikon Eclipse Ti Series inverted microscope with a C2 confocal
631 attachment, using the Immersion oil type F (Nikon) objective for the 100x lens. Analyses were
632 performed using the Nikon Elements Analysis 3.1 software.

633 Experiments with *Listeria Monocytogenes* (LM)

634 Recombinant LM expressing GP(33-41) epitope was a gift from Dr. Harty (University of Iowa). A
635 frozen aliquot of LM (stored at −80 °C) was thawed, cultured in Tryptic Soy Broth media (KD
636 Medical) with 50 μg/mL streptomycin, and optical density at 600 nm wavelength (OD600) was
637 measured hourly. OD600 of 1 corresponds to 1 x 10^9 CFU of LM. Once OD600 reached 0.08-
638 0.09, cells were spun down for 15 min at 6000 RPM, 4ºC and resuspended in 0.9% NaCl at the
639 concentration of 6 x 10^7 CFU/mL. Each recipient mouse was infected intravenously (i.v.) with 6 x
640 10^6 CFU of LM. Prior to infection but during the same day, mice were injected i.v. with 2 x 10^4
641 naïve $P14^+$ CD8 T cells.

642 Western blot analysis

643 Cells were collected and lysed in M2 lysis buffer (20mM Tris, pH7.0, 0.5% NP40, 250mM NaCl,
644 3mM EDTA, 3mM EGTA, 2mM DTT, 0.5mM PMSF, 20mM β-glycerol phosphate, 1mM sodium
645 vanadate, 1μg/mL Leupeptin), then resolved by SDS-PAGE. Blots were probed with anti-Dapl1,
646 anti-Zap70 (BD Biosciences), anti-HA (Cell Signaling) and anti-α-Tubulin (Sigma), and visualized

647 using enhanced chemiluminescence (ThermoScientific) with horse-radish peroxidase conjugated
648 anti-mouse IgG (Calbiochem) or anti-rabbit IgG (Jackson Immunoresearch).

649 Cloning, retroviral vectors and transduction

650 Open reading frames (ORF) of transcription factors (ID2, ID3, Klf2) and Dapl1 were PCR-
651 amplified using Phusion High-Fidelity DNA Polymerase (NEB) and ORF clones as templates
652 (Horizon Discoveries). The rest of transcription factors (Bcl11b, Foxo1, Bach2, Tcf7, Lef1, Klf2)
653 and HA-tagged Dapl1 constructs were synthesized (GenScript). Inserts were then cloned into
654 pMRX-IRES-GFP vector using NEBuilder HiFi DNA Assembly kit (NEB). Retroviruses were
655 produced from the transfection of Platinum-E cells with empty and gene-of-interest-expressing
656 pMRX-IRES-GFP vectors using the Transporter 5 transfection reagent (Polysciences) according
657 to the manufacturer's instructions. Viral supernatants were collected 24 hours after transfection,
658 concentrated with PEG-it (System Biosciences) and flash frozen in aliquots in liquid nitrogen. For
659 retroviral transduction of T cells, naïve lymphocytes were stimulated with irradiated splenocytes
660 in the presence of anti-CD3 mAbs (2 µg/mL) and irradiated splenocytes for 14 hours and then
661 spinfected (2000 RPM, 90 minutes, 37°C) with virus and polybrene (4 µg/mL). Media was
662 changed 4 hours after transduction, after which IL-2 was added at 100 U/mL daily until day 5 post
663 plating to generate CTLs. Jurkat cells were spinfected with virus and polybrene at 2000 RPM, 90
664 minutes, 37°C; NIH-3T3 cells were spinfected at 900 RPM, 90 minutes, 37°C.

665 Thymic egress inhibition experiments

666 Age and sex matched female Dapl1$^{ZsG/WT}$ mice were injected with 1mg/kg of the thymic egress
667 inhibitor FTY720 (Millipore Sigma) or with a 10% ethanol in PBS vehicle control intraperitoneally
668 every 48 hours for 8 days. Mice were sacrificed at day 9, and lymph nodes and spleens were
669 collected.

670 Isolation of RNA and quantitative PCR

671 RNA was isolated using The *Monarch* Total *RNA* Miniprep Kit (NEB). cDNA was synthesized
672 using the SensiFast cDNA Synthesis Kit (Thomas Scientific). SYBR Green quantitative PCR was

673 performed using the SensiFAST SYBR Lo-Rox kit (Thomas Scientific). SYBR Green primers
674 (Integrated DNA Technologies) used are as follows: Dapl1-F: ATGGCAAACGAAGTACAAGTTCT,
675 Dapl1-R: TCTTTCCAAAACGCCCATCTC, Rpl13A-F: CGAGGCATGCTGCCCCACAA, Rpl13A-
676 R: AGCAGGGACCACCATCCGCT.

677 Analysis of public RNAseq datasets

678 For reanalysis of bulk RNA sequencing data comparing Dapl1 expression in Bcl11b knockout
679 MPECs, normalized counts from GSE186283 were compared via an ordinary one-way ANOVA.
680 Graphs were generated via Graphpad Prism 10. For reanalysis of sorted thymic precursor data
681 (fig 6C), raw counts were obtained from GSE148973 [84]. Using the DESeq2 [95] package in R,
682 normalized counts and differential expression were calculated.

683 Analysis of public scRNAseq datasets

684 Single cell RNAseq Datasets were first screened for those that included clusters with a sufficient
685 amount of cells expressing *Dapl1* for calculating statistics. First, read count matrices were
686 downloaded from NCBI GEO, then analyzed using the Seurat package in R with standard
687 procedures, or with version 5.0 integration methods when appropriate. Next, cell clusters were
688 annotated based on the expression level of marker genes suggested by the original publications.
689 Finally, within respective clusters, differential gene expression was calculated between cells
690 expressing *Dapl1* at a level greater than 0.1 and cells expressing *Dapl1* at a level less than 0.1,
691 using the FindMarkers() function and the test="wilcox" option. For the meta-analysis of each cell
692 type of interest (naïve cells, Memory cells from acute infection, stem-like cells from TILs), the list
693 of differentially expressed genes were compared across different datasets and filtered for those
694 that were commonly upregulated or commonly downregulated in at least two datasets. The
695 intensity of differential expression of these genes were represented by plotting the average Log2
696 fold change values with the pheatmap package in R. Prediction of differentially enriched pathways
697 based on these genes were performed with Metascape [96], and the results were plotted using
698 ggplot2 package in R.

699 Datasets used for naïve cells: GSE131847 [71], GSE199563 [69], GSE213470 [72], GSE221969 [73],
700 GSE181784 [68], GSE186839 [70].
701 Datasets used for memory cells from acute infection models: GSE152841 [76], GSE131847 [71],
702 GSE182275 [75], GSE181784 [68], GSE119940 [62], GSE186839 [70].
703 Datasets used for Stem-like cells from tumors: E-MTAB-13073 [50], GSE180094 [6], GSE122712 [11],
704 GSE182509 [79], GSE221118 [81], GSE217038 [80].
705 For the multimodal thymic CITEseq dataset GSE186078 [85], the h5ad files were downloaded and
706 converted to a Seurat object in R. The FeaturePlot() function was used to visualize the expression
707 of select markers and differentiation pseudotime.
708 Statistical analysis
709 Data statistical analysis was performed with Prism 10 (GraphPad software). *P*-values for
710 comparisons of only two groups were determined using paired or unpaired two-tailed Student's *t*-
711 tests, with Mann-Whitney corrections if normal distributions could not be assumed. Ordinary
712 Brown-Forsythe and Welsh one-way ANOVAs comparisons were used to compare multiple
713 conditions, and two-way ANOVAs were used to compare tumor growth curves, cell population
714 proportions over time, and thymic egress inhibition experiments. Mixed effects analyses were
715 used to compare multiple groups of independently normalized data. Survival comparisons were
716 conducted using Kaplan-Meier tests. Sample size was not predetermined by statistical methods.
717 Two mice were excluded from analysis of day 30+ data from figure 5B due to signs of secondary
718 infection or malocclusion in adoptive transfer recipients; exclusion of these data points does not
719 impact the interpretation of results.
720
721
722
723
724

725 **Main Figures**

726 **Figure 1. (A)** Normalized *Dapl1* reads (FPKM) from RNAseq of WT (grey), Let7KD (red), and
727 Let7Tg (blue) CTLs (GSE232541). **(B)** Dapl1 expression (normalized by DESeq2) mined from the
728 ImmGen genome browser in TCRαβ T cell subsets. **(C)** Dapl1 protein expression (Western blot)
729 in total thymocytes, or CD4 or CD8 T cells from peripheral lymph nodes. **(D)** Confocal microscopy
730 of CD8 T cells stained for Dapl1 (red), CD8α (green), and DAPI (blue). **(E)** Representative flow
731 cytometric plots of lymphocytes taken from peripheral lymph nodes of B6 mice and intracellularly
732 stained for Dapl1. **(F)** Dapl1 expression by proportion (top) or MFI (bottom) in CD4 T cells (light
733 blue), CD8 T cells (blue), or $CD4^{-}CD8^{-}$ (DN, grey) cells from blood (n=6), spleen (n=3), or lymph
734 nodes (n=3) of B6 mice intracellularly stained for Dapl1. **(G)** UMAP projection of multicolor flow
735 cytometry data from splenic T cells of B6 mice clustered via Seurat. Splenocyte populations are
736 marked as CD4+Dapl1- (light grey), CD4+Dapl1+ (light blue), CD8+Dapl1- (dark grey), and
737 CD8+Dapl1+ (dark blue) T cells (n=3 per group). **(H)** Flow cytometric analysis of Dapl1-positive
738 or Dapl1-negative splenocytes using CD122 and CD44 as markers of differentiation (left), and
739 summary statistics of underlying splenocyte populations (right). **(I)** Surface protein expression on
740 naïve ($CD44^{low}CD62L^{high}$) T cells calculated either as MFI relative to the Dapl1- population (CD5,
741 CD44, CD62L, CD127, CD122) or as the proportion of Ly6C positive cells. Statistical analysis was
742 calculated using either an ordinary one-way ANOVA using Tukey's correction **(A, F top)**, two-
743 tailed unpaired *t*-tests **(F bottom)**, or two-tailed paired *t*-tests **(G, I)**. All data are representative of
744 three biological replicates from one RNA-seq analysis **(A)**, two or more independent experiments
745 **(B-G)**, or are pooled from three biological replicates from two independent experiments **(E-I)**.

746 **Figure 2. (A)** CRISPR-Cas9 mediated $Dapl1^{ZsG}$ reporter gene construct strategy, representing
747 introduction of P2A-ZsGreen to the end of Exon 4. **(B)** Representative flow cytometry plot of
748 lymphocytes from peripheral lymph nodes of $Dapl1^{ZsG/WT}$ mice (n=3, left). Data is summarized by
749 proportion or MFI in CD4 T cells (light green), CD8 T cells (green), or $CD4^{-}CD8^{-}$ (DN, grey) cells
750 (right). **(C)** Western blot analysis of Dapl1 and Zap70 expression in whole cell lysates from CD8
751 T cells enriched from lymph nodes of WT, $Dapl1^{ZsG/WT}$, or $Dapl1^{ZsG/ZsG}$ mice. **(D)** Representative
752 UMAP projection (left) of multicolor flow cytometry data from spleen of $Dapl1^{ZsG/WT}$ mice clustered
753 via Seurat. ZsGreen expression is represented as both a featureplot (middle) or violin plots split
754 by cell subset (right). **(E)** Representative flow cytometry plots of splenocytes from
755 $Dapl1^{ZsG/WT}FoxP3^{RFP/RFP}$ mice. **(F-K)** Proportion of ZsGreen expressing cells within **(F)** spleen, **(G)**
756 liver and **(H)** gut subsets: small intestine intraepithelial lymphocyte (IEL), small intestine lamina
757 propria lymphocyte (LPL), colon IEL, or colon LPL. All statistical analysis was calculated using
758 ordinary one-way ANOVAs with Tukey's correction for multiple comparisons. All data are
759 representative of more than three independent experiments **(B,E,F)**, one experiment **(C-D)**, three
760 biological replicates from one experiment **(G)**, or at least two biological replicates pooled from
761 three independent experiments **(H-K)**.

762 **Figure 3. (A)** Representative UMAP projection of multicolor flow cytometry data from splenic T
763 cells of $Dapl1^{ZsG/WT}Foxp3^{RFP/RFP}$ mice clustered via Seurat. Splenocyte populations are marked as
764 CD4+ZsG- (light grey), CD4+ZsG+ (light green), CD8+ZsG- (grey), CD8+ZsG+ (dark green),
765 ZsG-Tregs (dark grey), and ZsG+Tregs (red). **(B)** Flow cytometric analysis of ZsGreen-positive
766 or ZsGreen-negative splenocytes using CD122 and CD44 as markers of differentiation (left), and
767 summary statistics of underlying splenocyte populations (right). **(C)** Summary statistics of
768 individual surface marker expression on naïve ($CD44^{low}CD62L^{high}$) T cells, calculated either as
769 MFI relative to the ZsGreen- population (CD5, CD44, CD62L, CD127) or as the proportion of

770 Ly6C-positive cells. **(D)** Representative flow cytometry plots demonstrating heterogeneity of
771 Dapl1 expression among circulating WT Dapl1$^{ZsG/WT}$, Dapl1$^{ZsG/WT}$P14^{+}Rag2$^{-/-}$, or
772 Dapl1$^{ZsG/WT}$OTI^{+}Rag2$^{-/-}$ CD8 T cells. **(E)** ScRNAseq analysis of naïve CD8 T cells from P14^{+}Rag2^{-}
773 $^{/-}$, OTI^{+}Rag2$^{-/-}$, or WT datasets (GSE131847, GSE199563, GSE213470, GSE221969,
774 GSE181784, GSE186839), consisting of (top) violin plots representing Dapl1 heterogeneity,
775 (middle) descriptions of the datasets, and (bottom) a heatmap of consistently differentially
776 expressed genes among datasets. **(F)** Pathway enrichment analysis denoting significantly
777 different pathways between Dapl1 positive and Dapl1 negative naïve CD8 T cells. Statistical
778 analysis for **(B, C)** was calculated via two-tailed paired *t* tests for difference. All data are pooled
779 from three biological replicates from at least two independent experiments **(A-C)**, or
780 representative of at least three independent experiments **(D)**.

781

782 **Figure 4. (A)** Schematic of P14^{+}Rag2$^{-/-}$ CD8 T cell differentiation into CTLs (top left).
783 Representative flow cytometry plots of Dapl1 expression on day 5 CTLs (bottom left). Proportions
784 of CD62L^{+}Tim3^{-} or CD62L^{-}Tim3^{+} cells in Dapl1- and Dapl1+ populations (bottom middle) and MFI
785 fold change of surface markers relative to Dapl1- cells (n = 3, bottom right). **(B)** ZsGreen
786 expression in day 5 CTLs from Dapl1$^{ZsG/WT}$P14^{+}Rag2$^{-/-}$ reporter mice (left). Proportions of
787 CD62L^{+}Tim3^{-} or CD62L^{-}Tim3^{+} cells in ZsGreen^{-} and ZsGreen^{+} populations (middle) and MFI fold
788 changes of surface markers relative to ZsGreen^{-} cells (n = 2, right). **(C)** Proportions of ZsGreen^{+}
789 CTLs when differentiated with DMSO or rapamycin-supplemented media for the first 48h of
790 activation (n = 3). **(D)** Schematic of LM-GP33 challenge and adoptive T cell transfer (top). Flow
791 cytometry plots of ZsGreen expression at days 0, 7, 14 (blood), and 30+ (spleen) post-infection
792 (n = 8, left). Temporal changes in population proportions over time: ZsGreen^{-} sorted cells which
793 continued to be ZsGreen^{-} (ZsG-, grey), ZsGreen^{+} cells within the ZsGreen^{-} sorted group (*De novo*,
794 black), sorted cells which lost ZsGreen expression (Ex-ZsG, purple), and cells which retained
795 ZsGreen (ZsG+, green, right). **(E)** Surface expression of KLRG1 vs CD127 and CD62L vs CD44
796 on CD8 T cells at days 7, 14 (blood), and 30 (spleen) (left). Frequencies of SLECs, INT, MPECs,
797 effector memory, and central memory within ZsG-, Ex- ZsG, and ZsG+ groups (n = 8, right). **(F)**
798 Analysis of publicly available scRNAseq datasets of memory CD8 T cells generated via LCMV
799 Armstrong (Arm) (GSE152841, GSE131847, GSE182275, GSE181784, GSE119940) or
800 influenza A virus (IAV) (GSE186839), consisting of (top) violin plots representing *Dapl1*
801 heterogeneity, (middle) descriptions of the datasets, and (bottom) a heatmap of consistently
802 differentially expressed genes among datasets. **(G)** Proportions of Dapl1+, CD62L+Tim3-, or
803 CD62L-Tim3+ CTLs by intracellular staining following transcription factor overexpression with
804 GFP-tagged vectors, presented as fold change in GFP+ vs. GFP− cells (n = 3). Statistical analysis
805 was calculated using two-tailed paired *t*-tests **(A, B),** a two-tailed unpaired *t*-test **(C)**, ordinary two-
806 way ANOVA with FDR correction **(D)**, ordinary one-way ANOVAs using Tukey's correction **(E),** or
807 ordinary one-way ANOVAs using Dunnet's correction **(G)**. Data are representative of two or more
808 independent experiments (**A-D**) or are pooled from three independent experiments (**G**).

809 **Figure 5. (A)** Experimental design of LM-GP33 challenge and adoptive T cell transfer(top).
810 Representative flow cytometry plots of Dapl1 or ZsGreen expression in adoptively transferred
811 P14^{+}Rag2$^{-/-}$ or Dapl1$^{ZsG/ZsG}$P14^{+}Rag2$^{-/-}$ CD8 T cells at days 0, 7, or 14 post-infection in the blood
812 and day 30+ in the spleen (left), with dynamic changes in proportions of WT Dapl1+ (blue) or
813 Dapl1-wannabe (peach) cells over time (right). **(B)** Representative flow cytometry plots of the
814 surface expression of KLRG1 vs CD127 (Day 7, 14) and CD62L vs CD44 (Day 30+) on CD8 T

cells at day 7 and 14 post-infection in the blood and day 30 in the spleen (left). Quantification of the frequencies of KLRG1^{+}CD127^{-} (SLECs), KLRG1^{+}CD127^{+} (intermediate (INT), KLRG1^{-}CD127^{+} (MPECs), CD62L^{+}CD44^{-} (effector memory), and CD62L^{+}CD44^{+} (central memory) populations within Dapl1-negative, Dapl1-positive, ZsGreen-negative, and Dapl1-wannabe populations (right). **(C)** Representative flow cytometry plots of TNFα and IFNγ secretion of day 30+ memory CD8 T cells 4 hours post stimulation with ionomycin and PMA (left), with quantification (right). All summary plots are pooled from 12 (WT) and 13 (Dapl1$^{ZsG/ZsG}$) biological replicates at days 7 and 14, and 8 biological replicates at day 30+ for both groups from three independent experiments **(A-B)**, or 8 (WT) or 6 (Dapl1$^{ZsG/ZsG}$) biological replicates pooled from two independent experiments **(C)**. Statistical analyses were conducted via ordinary two-way ANOVA with FDR correction **(A)**, Brown-Forsythe and Welsh ANOVA tests **(B),** or a mixed-effects analysis with Šidák's correction **(C)**.

Figure 6. (A) Flow cytometry plots of FoxP3 and ZsGreen expression on splenocytes from one-day (n = 4), one-week (n = 4), or one-month (n =3) old Dapl1$^{ZsG/WT}$FoxP3$^{RFP/RFP}$ mice (left), with quantification of ZsGreen expression among CD4 (light green), CD8 (dark green), and Treg (red) subsets (right). **(B)** Expression of ZsGreen in Dapl1$^{ZsG/WT}$ mice on mature thymic CD4 and CD8 populations, as marked by TCRβ (left), with summary (right). **(C)** *Dapl1* expression by RNAseq of thymic subsets sorted by maturity from (top, GSE148973), with heatmap of defining characteristics by subset (bottom). **(D)** UMAP plots regenerated from the multimodal dataset (GSE186078) denoting pseudotime, *Cd4*, *Cd8*, and *Dapl1* expression. **(E)** Flow cytometry histogram of surface CD24 expression in CD8α^{+} cells from the thymus or lymph nodes of Dapl1$^{ZsG/WT}$ mice stratified by ZsGreen expression (left), with summary (right). **(F)** ZsGreen MFI in CD8α^{+} cells from the thymus or lymph nodes of Dapl1$^{ZsG/WT}$ mice (n=3). **(G)** Flow cytometry plots denoting ZsGreen expression in thymocytes from Dapl1$^{ZsG/WT}$ mice treated with daily IP injections of either ethanol (n=2) or FTY720 (n=3), with summary of replicates (right). All data are representative of two to four biological replicates from one experiment **(A,G)**, or are representative of at least two independent experiments **(B,E,F)**. Statistical analysis was conducted using either an ordinary two-way ANOVAs using Tukey's correction **(A,G)**, matched one-way Anova with Geisser-Greenhouse correction **(B)**, DESEQ2 **(C)**, one-way Welsh's Anova **(E)**, or two-tailed unpaired *t* test **(F)**.

855 **Supplementary Figures**

856 **Figure S1. (A)** ELISA verification of anti-Dapl1 clone 6H9 monoclonal antibodies (n=8 per group).
857 Each dot represents a well of a 96-well plate. **(B)** Protein expression (Western blot) of Dapl1 in
858 3T3 cells transduced with either an empty-pMRX or Dapl1-pMRX virus, using anti-Dapl1 clone
859 6H9 antibodies. **(C)** Confocal microscopy of 3T3 cells transduced with either an empty-pMRX or
860 Dapl1-pMRX virus and stained for Dapl1. Dapl1 staining is shown with red, GFP with green, and
861 DAPI with blue. **(D)** Violin plots of underlying expression patterns of all protein markers in
862 splenocytes used for clustering in figure 1G. **(E)** Gating schema and expression patterns of CD62L
863 and CD44 used for figure 1H to define naïve and differentiated T cells. **(F)** Representative
864 histograms of surface marker expression on naïve splenocytes used to generate Figure 1I
865 summary plots. Data are either pooled from three independent experiments **(A)**, from a single
866 experiment **(B)**, or representative of at least two independent experiments **(C-F)**. Statistical
867 analysis for **(A)** was calculated using a two-tailed unpaired *t* test.

868 **Figure S2. (A).** Initial population proportions and post-sort purity of ZsGreen- or ZsGreen+ cells
869 from CD8 T cells collected from lymph nodes of Dapl1$^{ZsG/ZsG}$ mice and sorted by ZsGreen
870 expression (left), followed by expression of Dapl1 mRNA as detected by qPCR (right). **(B)** Protein
871 expression of Dapl1 (Western blot) in untransduced Jurkat cells, Jurkat cells overexpressing
872 modified N-terminus HA tagged Dapl1 (HA-Dapl1), or Jurkat cells overexpressing modified C-
873 terminus HA tagged Dapl1 (Dapl1-HA). **(C)** Violin plots of surface protein expression of all markers
874 analyzed for the splenic immune populations characterized in Figure 2D. Data are representative
875 of at least two independent experiments **(A)**, or one experiment **(B,C)**.

876 **Figure S3. (A)** Gating strategies and representative plots used to characterize T cell populations
877 in the spleen of Dapl1$^{ZsG/WT}$ mice, as summarized in Fig. 2F. **(B)** Gating strategies and
878 representative plots used to characterize T cell populations in the liver of Dapl1$^{ZsG/WT}$ mice, as
879 summarized in Figure 2G. All data are representative of three or more biological replicates.

880 **Figure S4. (A-D)** Gating strategies and representative flow cytometry plots used to characterize
881 T cell populations in **(A)** small intestine IELs, **(B)** small intestine LPLs, **(C)** colon IELs, or **(D)** colon
882 LPLs of Dapl1$^{ZsG/WT}$ mice, as summarized in Figure 2 H. All data are representative of 2-3
883 biological replicates from three independent experiments.

884 **Figure S5. (A)** Violin plots of surface protein expression of all markers analyzed for the splenic
885 immune populations characterized in Figure 3A. **(B)** Gating strategy and representative flow
886 cytometry plots used to identify CD4^{+}FoxP3^{RFP-}, CD4^{+}FoxP3^{RFP+}, CD8α^{+}FoxP3^{RFP-},
887 CD8α^{+}FoxP3^{RFP+} T cell populations in spleens of Dapl1$^{ZsG/WT}$ FoxP3$^{RFP/RFP}$ mice **(C)**
888 Representative flow cytometry histograms of surface proteins on naïve (CD44^{low}CD62L^{high}) CD4
889 and CD8 T cells from Dapl1$^{ZsG/WT}$ FoxP3$^{RFP/RFP}$ mice. **(D)** Representative flow cytometry
890 histograms of surface proteins on CD4^{+}FoxP3^{RFP+} T regulatory cells from Dapl1$^{ZsG/WT}$FoxP3$^{RFP/RFP}$
891 mice**.** Summary statistics of individual surface marker expression on CD4^{+}FoxP3^{RFP+} T regulatory
892 cells from Dapl1$^{ZsG/WT}$FoxP3$^{RFP/RFP}$ mice, calculated either as MFI relative to the ZsGreen-
893 population or as the proportion of ZsGreen positive or negative cells which express the indicated
894 marker. All data are representative of three biological replicates from two independent
895 experiments **(C)**. All statistical analysis was conducted using two-tailed paired *t* tests for
896 difference.

897 **Figure S6. (A-B)** Representative flow cytometry histograms of surface markers on CTLs
898 differentiated either from **(A)** WT $P14^{+}Rag2^{-/-}$ or **(B)** $Dapl1^{ZsG/WT}P14^{+}Rag2^{-/-}$ CD8 T cells. **(C)**
899 Experimental design and representative surface marker expression from $Dapl1^{ZsG/WT}P14^{+}Rag2^{-/-}$
900 CD8 T cells sorted by ZsGreen expression and differentiated into CTLs. **(D)** Total number of CD8
901 T cells collected from spleens and lymph nodes of mice 30+ days post adoptive transfer of
902 $Dapl1^{ZsG/WT}P14^{+}Rag2^{-/-}$ CD8 T cells sorted by ZsGreen expression, followed by LM-GP33
903 challenge (n=8 per group). **(E)** CD62L surface expression on sorted CD8 T cells at day 7 and 14
904 post-infection in the blood and day 30^{+} in the spleen (n=8 per group). **(F)** ScRNAseq clustering of
905 memory CD8 T cell subsets from GSE181784, with *Dapl1* expression marked in blue (right). **(G)**
906 Pathways enriched by genes upregulated (orange) or downregulated (blue) in *Dapl1*$^{+}$ memory
907 CD8 T cells generated via LCMV Armstrong (Arm) (GSE152841, GSE131847, GSE182275,
908 GSE181784, GSE119940) or influenza A virus (IAV) (GSE186839). All data are representative of
909 three biological replicates (**A**), two biological replicates (**B**), three independent experiments (**C**),
910 or two independent experiments (**D-E**). Statistical analyses were conducted using an unpaired
911 two-tailed *t* test (**D**), or an ordinary one-way Anova with Tukey's correction (**E**).

912 **Figure S7. (A)** Proposed model of naïve T cell differentiation, where a subset of Dapl1+ cells
913 (marked in red) is maintained exclusively in the memory lineage.

914 Figure S8. **(A)** Representative flow cytometry plots of $P14^{+}Rag2^{-/-}$ CD8 T cells transduced with
915 GFP-reported transcription factor overexpression vectors, demonstrating transduction efficiency
916 (left), and Dapl1 (middle) or Tim3, and CD62L protein levels (right) stratified by GFP expression.
917 **(B)** Bulk RNAseq analysis of sorted CD8 T cell MPECs ($KLRG1^{-}CD127^{+}$) or SLECs
918 ($KLRG1^{+}CD127^{-}$) day 9 post LM-OVA challenge from either $Bcl11b^{-/-}$ or WT mice (GSE186283).
919 Data are representative of three independent experiments **(A)**, or one bulk RNA sequencing
920 dataset with three biological replicates (**B**).

921 **Figure S9. (A)** Schema of tumor infiltrating lymphocyte (TIL) experiment (top), with Tim3 and
922 CD62L surface expression on Dapl1- or Dapl1+ TILs at day 8 post B16 melanoma implantation
923 into WT mice (bottom). CD45.2 was injected into mice before sacrifice to minimize contamination
924 of circulating cells in analysis (n=6 tumors). **(B)** Representative histograms denoting CD44
925 surface expression on tumor draining lymph nodes (TDLNs), TILs, and $CD45.2^{+}$ contamination of
926 day 8 WT TILs intracellularly stained for Dapl1. **(C)** Experimental schema (top) and summary
927 proportions (bottom) of $CD62L^{-}Tim3^{+}$ and $CD62L^{+}Tim3^{-}$ surface expression on ZsG+ or ZsG- TILs
928 at day 8 post B16 melanoma implantation into $Dapl1^{ZsG/WT}$ mice, as well as Ly108 MFI normalized
929 to the average Ly108 MFI of ZsG- cells. (**D**) scRNAseq analysis of tumor infiltrating CD8 T cells
930 (E-MTAB-13073), indicating Dapl1 expression in Tpex and Tex subsets. **(E)** ScRNAseq analysis
931 of tumor infiltrating CD8 T cells from publicly available datasets (E-MTAB-13073, GSE180094,
932 GSE122712, GSE182509, GSE221118, GSE217038), consisting of (top) violin plots representing
933 *Dapl1* heterogeneity in stem-like TILs, (middle) descriptions of the datasets, and (bottom) a
934 heatmap of consistently differentially expressed genes among datasets. **(F)** Pathways enriched
935 by genes upregulated (orange) or downregulated (blue) in *Dapl1*$^{+}$ versus *Dapl1*$^{-}$ stem-like TILs.
936 Data are either pooled from two independent experiments **(A, C)**, or are from one experiment **(B)**.
937 All statistical analysis of flow cytometry data was conducted via two-tailed unpaired *t* tests.

938 **Figure S10. (A)** CD62L surface expression on WT $P14^{+}Rag2^{-/-}$ or $Dapl1^{ZsG/ZsG}P14^{+}Rag2^{-/-}$ CD8 T
939 cells at day 7 and 14 post-LM-GP33 infection in the blood and day 30^{+} in the spleen, stratified by
940 Dapl1 or ZsGreen expression. **(B)** Schematic of $Dapl1^{ZsG/ZsG}P14^{+}Rag2^{-/-}$ CD8 T cell differentiation
941 into CTLs (top). Representative flow cytometry plots of ZsG expression on day 5 CTLs (left).

Proportions of CD62L^{+}Tim3^{-} or CD62L^{-}Tim3^{+} cells in ZsG- and ZsG+ populations (right). **(C)** Experimental schema (top), representative flow cytometry plots (left), and summary proportions (right) of CD62L^{-}Tim3^{+} and CD62L^{+}Tim3^{-} surface expression on ZsG+ or ZsG- TILs at day 8 post B16 melanoma implantation into Dapl1$^{ZsG/ZsG}$ mice. **(D)** Efficiency of Dapl1-mCherry and Empty-mCherry viruses on cultured CD8 T cells 24 hours after transduction (left). Proportions and phenotypes of Dapl1-mCherry and Empty-mCherry positive cells 7 days after adoptive transfer into Rag2$^{-/-}$ hosts and LM-GP33 infection (middle), with summary statistics (right). **(E)** Experimental schema of sort and adoptive transfer of memory CD8 T cells into B6 hosts 30+ days post LM-GP33 priming to treat B16-GD33 melanoma (top), with tumor growth curves (left) and survival curves (right). **(F)** Experimental schema of MC38 tumor challenge of WT, Dapl1$^{ZsG/WT}$, and Dapl1$^{ZsG/ZsG}$ hosts (top), with tumor growth curves (left) and survival curves (right). Statistical analysis was conducted using either a mixed-effect analysis **(A)**, two-tailed paired *t* tests for difference **(B)**, or two-way ANOVAs **(D-F)**. All survival analysis was conducted using Kaplan-Meier's test. Data are either pooled from three independent experiments **(A)**, pooled from four independent experiments **(B)**, or are from one experiment **(C-F)**.

Figure S11. (A) Gating strategies and representative flow cytometry plots used to characterize T cell populations in the thymus of Dapl1$^{ZsG/WT}$ mice, with summary information (n=3). **(B)** Flow cytometry plots denoting ZsGreen expression in T cells derived from lymph nodes of Dapl1$^{ZsG/WT}$ mice treated with daily IP injections of either ethanol (n=2) or FTY720 (n=3), with summary of replicates (right). Statistical analysis was conducted using either an ordinary one-way ANOVA (**A**) or an ordinary two-way ANOVAs using Tukey's correction (**B**).

977 **References**

978 1. Blackburn, S.D., Shin, H., Freeman, G.J. & Wherry, E.J. Selective expansion of a subset
979 of exhausted CD8 T cells by alphaPD-L1 blockade. *Proc Natl Acad Sci U S A* **105**,
980 15016-21 (2008).
981 2. Chang, J.T., Wherry, E.J. & Goldrath, A.W. Molecular regulation of effector and memory
982 T cell differentiation. *Nat Immunol* **15**, 1104-15 (2014).
983 3. Gebhardt, T., Park, S.L. & Parish, I.A. Stem-like exhausted and memory CD8(+) T cells
984 in cancer. *Nat Rev Cancer* **23**, 780-798 (2023).
985 4. Geiger, R. *et al.* L-Arginine Modulates T Cell Metabolism and Enhances Survival and
986 Anti-tumor Activity. *Cell* **167**, 829-842 e13 (2016).
987 5. Huang, A.C. *et al.* T-cell invigoration to tumour burden ratio associated with anti-PD-1
988 response. *Nature* **545**, 60-65 (2017).
989 6. Huang, Q. *et al.* The primordial differentiation of tumor-specific memory CD8(+) T cells
990 as bona fide responders to PD-1/PD-L1 blockade in draining lymph nodes. *Cell* **185**,
991 4049-4066 e25 (2022).
992 7. Im, S.J. *et al.* Defining CD8+ T cells that provide the proliferative burst after PD-1
993 therapy. *Nature* **537**, 417-421 (2016).
994 8. Kallies, A., Zehn, D. & Utzschneider, D.T. Precursor exhausted T cells: key to successful
995 immunotherapy? *Nat Rev Immunol* **20**, 128-136 (2020).
996 9. Krishna, S. *et al.* Stem-like CD8 T cells mediate response of adoptive cell
997 immunotherapy against human cancer. *Science* **370**, 1328-1334 (2020).
998 10. LaFleur, M.W. *et al.* PTPN2 regulates the generation of exhausted CD8(+) T cell
999 subpopulations and restrains tumor immunity. *Nat Immunol* **20**, 1335-1347 (2019).
1000 11. Miller, B.C. *et al.* Subsets of exhausted CD8(+) T cells differentially mediate tumor
1001 control and respond to checkpoint blockade. *Nat Immunol* **20**, 326-336 (2019).
1002 12. Sade-Feldman, M. *et al.* Defining T Cell States Associated with Response to Checkpoint
1003 Immunotherapy in Melanoma. *Cell* **175**, 998-1013 e20 (2018).
1004 13. Siddiqui, I. *et al.* Intratumoral Tcf1(+)PD-1(+)CD8(+) T Cells with Stem-like Properties
1005 Promote Tumor Control in Response to Vaccination and Checkpoint Blockade
1006 Immunotherapy. *Immunity* **50**, 195-211 e10 (2019).
1007 14. Thommen, D.S. *et al.* A transcriptionally and functionally distinct PD-1(+) CD8(+) T cell
1008 pool with predictive potential in non-small-cell lung cancer treated with PD-1 blockade.
1009 *Nat Med* **24**, 994-1004 (2018).
1010 15. Wells, A.C. *et al.* Let-7 enhances murine anti-tumor CD8 T cell responses by promoting
1011 memory and antagonizing terminal differentiation. *Nat Commun* **14**, 5585 (2023).
1012 16. Zehn, D., Thimme, R., Lugli, E., de Almeida, G.P. & Oxenius, A. 'Stem-like' precursors
1013 are the fount to sustain persistent CD8(+) T cell responses. *Nat Immunol* **23**, 836-847
1014 (2022).
1015 17. Ahmed, R., Bevan, M.J., Reiner, S.L. & Fearon, D.T. The precursors of memory: models
1016 and controversies. *Nat Rev Immunol* **9**, 662-8 (2009).
1017 18. Akondy, R.S. *et al.* Origin and differentiation of human memory CD8 T cells after
1018 vaccination. *Nature* **552**, 362-367 (2017).
1019 19. Buchholz, V.R., Schumacher, T.N. & Busch, D.H. T Cell Fate at the Single-Cell Level.
1020 *Annu Rev Immunol* **34**, 65-92 (2016).
1021 20. Chang, J.T. *et al.* Asymmetric T lymphocyte division in the initiation of adaptive immune
1022 responses. *Science* **315**, 1687-91 (2007).
1023 21. Gerlach, C. *et al.* Heterogeneous differentiation patterns of individual CD8+ T cells.
1024 *Science* **340**, 635-9 (2013).
1025 22. Guo, A. *et al.* cBAF complex components and MYC cooperate early in CD8(+) T cell
1026 fate. *Nature* **607**, 135-141 (2022).

1027 23. Kaech, S.M. & Ahmed, R. Memory CD8+ T cell differentiation: initial antigen encounter
1028 triggers a developmental program in naive cells. *Nat Immunol* **2**, 415-22 (2001).
1029 24. Kakaradov, B. *et al.* Early transcriptional and epigenetic regulation of CD8(+) T cell
1030 differentiation revealed by single-cell RNA sequencing. *Nat Immunol* **18**, 422-432 (2017).
1031 25. Mercado, R. *et al.* Early programming of T cell populations responding to bacterial
1032 infection. *J Immunol* **165**, 6833-9 (2000).
1033 26. Stemberger, C. *et al.* A single naive CD8+ T cell precursor can develop into diverse
1034 effector and memory subsets. *Immunity* **27**, 985-97 (2007).
1035 27. Verbist, K.C. *et al.* Metabolic maintenance of cell asymmetry following division in
1036 activated T lymphocytes. *Nature* **532**, 389-93 (2016).
1037 28. Deep, D. *et al.* Precursor central memory versus effector cell fate and naive CD4+ T cell
1038 heterogeneity. *J Exp Med* **221**(2024).
1039 29. Eggert, J. & Au-Yeung, B.B. Functional heterogeneity and adaptation of naive T cells in
1040 response to tonic TCR signals. *Curr Opin Immunol* **73**, 43-49 (2021).
1041 30. Hale, B.D. *et al.* Cellular architecture shapes the naive T cell response. *Science* **384**,
1042 eadh8697 (2024).
1043 31. Ju, Y.J. *et al.* Self-reactivity controls functional diversity of naive CD8(+) T cells by co-
1044 opting tonic type I interferon. *Nat Commun* **12**, 6059 (2021).
1045 32. Li, J. *et al.* KIR(+)CD8(+) T cells suppress pathogenic T cells and are active in
1046 autoimmune diseases and COVID-19. *Science* **376**, eabi9591 (2022).
1047 33. Rogers, D. *et al.* Pre-existing chromatin accessibility and gene expression differences
1048 among naive CD4(+) T cells influence effector potential. *Cell Rep* **37**, 110064 (2021).
1049 34. Rudd, B.D. Neonatal T Cells: A Reinterpretation. *Annu Rev Immunol* **38**, 229-247
1050 (2020).
1051 35. Bartleson, J.M. *et al.* Strength of tonic T cell receptor signaling instructs T follicular
1052 helper cell-fate decisions. *Nat Immunol* **21**, 1384-1396 (2020).
1053 36. ElTanbouly, M.A. *et al.* VISTA is a checkpoint regulator for naive T cell quiescence and
1054 peripheral tolerance. *Science* **367**(2020).
1055 37. Mandl, J.N., Monteiro, J.P., Vrisekoop, N. & Germain, R.N. T cell-positive selection uses
1056 self-ligand binding strength to optimize repertoire recognition of foreign antigens.
1057 *Immunity* **38**, 263-274 (2013).
1058 38. Persaud, S.P., Parker, C.R., Lo, W.L., Weber, K.S. & Allen, P.M. Intrinsic CD4+ T cell
1059 sensitivity and response to a pathogen are set and sustained by avidity for thymic and
1060 peripheral complexes of self peptide and MHC. *Nat Immunol* **15**, 266-74 (2014).
1061 39. Weber, K.S. *et al.* Distinct CD4+ helper T cells involved in primary and secondary
1062 responses to infection. *Proc Natl Acad Sci U S A* **109**, 9511-6 (2012).
1063 40. Chen, H.B. *et al.* DAPL1 is a novel regulator of testosterone production in Leydig cells of
1064 mouse testis. *Sci Rep* **11**, 18532 (2021).
1065 41. Grassmann, F. *et al.* A Candidate Gene Association Study Identifies DAPL1 as a
1066 Female-Specific Susceptibility Locus for Age-Related Macular Degeneration (AMD).
1067 *Neuromolecular Med* **17**, 111-20 (2015).
1068 42. Hattori, Y. *et al.* Attenuation of growth hormone production at the fetal stage is critical for
1069 dioxin-induced developmental disorder in rat offspring. *Biochem Pharmacol* **186**, 114495
1070 (2021).
1071 43. Ma, X. *et al.* DAPL1 prevents epithelial-mesenchymal transition in the retinal pigment
1072 epithelium and experimental proliferative vitreoretinopathy. *Cell Death Dis* **14**, 158
1073 (2023).
1074 44. Ma, X. *et al.* DAPL1, a susceptibility locus for age-related macular degeneration, acts as
1075 a novel suppressor of cell proliferation in the retinal pigment epithelium. *Hum Mol Genet*
1076 **26**, 1612-1621 (2017).

1077 45. Zhu, L. *et al.* Dapl1 controls NFATc2 activation to regulate CD8(+) T cell exhaustion and
1078 responses in chronic infection and cancer. *Nat Cell Biol* **24**, 1165-1176 (2022).
1079 46. Leesch, F. *et al.* A molecular network of conserved factors keeps ribosomes dormant in
1080 the egg. *Nature* **613**, 712-720 (2023).
1081 47. Ma, X. *et al.* DAPL1 deficiency in mice impairs antioxidant defenses in the RPE and
1082 leads to retinal degeneration with AMD-like features. *Redox Biol* **62**, 102675 (2023).
1083 48. Baharom, F. *et al.* Intravenous nanoparticle vaccination generates stem-like TCF1(+)
1084 neoantigen-specific CD8(+) T cells. *Nat Immunol* **22**, 41-52 (2021).
1085 49. Carmona, S.J., Siddiqui, I., Bilous, M., Held, W. & Gfeller, D. Deciphering the
1086 transcriptomic landscape of tumor-infiltrating CD8 lymphocytes in B16 melanoma tumors
1087 with single-cell RNA-Seq. *Oncoimmunology* **9**, 1737369 (2020).
1088 50. Castiglioni, A. *et al.* Combined PD-L1/TGFbeta blockade allows expansion and
1089 differentiation of stem cell-like CD8 T cells in immune excluded tumors. *Nat Commun* **14**,
1090 4703 (2023).
1091 51. Chen, A.C.Y. *et al.* The aged tumor microenvironment limits T cell control of cancer. *Nat*
1092 *Immunol* **25**, 1033-1045 (2024).
1093 52. Dean, J.W. *et al.* The aryl hydrocarbon receptor cell intrinsically promotes resident
1094 memory CD8(+) T cell differentiation and function. *Cell Rep* **42**, 111963 (2023).
1095 53. Highton, A.J. *et al.* Single-cell transcriptome analysis of CD8 (+) T-cell memory inflation.
1096 *Wellcome Open Res* **4**, 78 (2019).
1097 54. Hou, S. *et al.* Virtual memory T cells orchestrate extralymphoid responses conducive to
1098 resident memory. *Sci Immunol* **6**, eabg9433 (2021).
1099 55. Lan, X. *et al.* Antitumor progenitor exhausted CD8(+) T cells are sustained by TCR
1100 engagement. *Nat Immunol* **25**, 1046-1058 (2024).
1101 56. Pauken, K.E. *et al.* Single-cell analyses identify circulating anti-tumor CD8 T cells and
1102 markers for their enrichment. *J Exp Med* **218**(2021).
1103 57. Roychoudhuri, R. *et al.* Transcriptional profiles reveal a stepwise developmental
1104 program of memory CD8(+) T cell differentiation. *Vaccine* **33**, 914-23 (2015).
1105 58. Tsui, C. *et al.* MYB orchestrates T cell exhaustion and response to checkpoint inhibition.
1106 *Nature* **609**, 354-360 (2022).
1107 59. Van Der Byl, W. *et al.* The CD8(+) T cell tolerance checkpoint triggers a distinct
1108 differentiation state defined by protein translation defects. *Immunity* **57**, 1324-1344 e8
1109 (2024).
1110 60. Vokali, E. *et al.* Lymphatic endothelial cells prime naive CD8(+) T cells into memory cells
1111 under steady-state conditions. *Nat Commun* **11**, 538 (2020).
1112 61. Yao, C. *et al.* BACH2 enforces the transcriptional and epigenetic programs of stem-like
1113 CD8(+) T cells. *Nat Immunol* **22**, 370-380 (2021).
1114 62. Yao, C. *et al.* Single-cell RNA-seq reveals TOX as a key regulator of CD8(+) T cell
1115 persistence in chronic infection. *Nat Immunol* **20**, 890-901 (2019).
1116 63. Zou, D. *et al.* CD4(+) T cell immunity is dependent on an intrinsic stem-like program. *Nat*
1117 *Immunol* **25**, 66-76 (2024).
1118 64. Heng, T.S., Painter, M.W. & Immunological Genome Project, C. The Immunological
1119 Genome Project: networks of gene expression in immune cells. *Nat Immunol* **9**, 1091-4
1120 (2008).
1121 65. Azzam, H.S. *et al.* Fine tuning of TCR signaling by CD5. *J Immunol* **166**, 5464-72
1122 (2001).
1123 66. Delpoux, A. *et al.* TCR signaling events are required for maintaining CD4 regulatory T
1124 cell numbers and suppressive capacities in the periphery. *J Immunol* **193**, 5914-23
1125 (2014).
1126 67. Lee, J.Y. *et al.* Phenotypic and Functional Changes of Peripheral Ly6C(+) T Regulatory
1127 Cells Driven by Conventional Effector T Cells. *Front Immunol* **9**, 437 (2018).

1128 68. Chen, Y., Shen, J., Kasmani, M.Y., Topchyan, P. & Cui, W. Single-Cell Transcriptomics
1129 Reveals Core Regulatory Programs That Determine the Heterogeneity of Circulating and
1130 Tissue-Resident Memory CD8(+) T Cells. *Cells* **10**(2021).
1131 69. Giles, J.R. *et al.* Shared and distinct biological circuits in effector, memory and
1132 exhausted CD8(+) T cells revealed by temporal single-cell transcriptomics and
1133 epigenetics. *Nat Immunol* **23**, 1600-1613 (2022).
1134 70. Guo, K. *et al.* The chemokine receptor CXCR3 promotes CD8(+) T cell-dependent lung
1135 pathology during influenza pathogenesis. *Sci Adv* **10**, eadj1120 (2024).
1136 71. Kurd, N.S. *et al.* Early precursors and molecular determinants of tissue-resident memory
1137 CD8(+) T lymphocytes revealed by single-cell RNA sequencing. *Sci Immunol* **5**(2020).
1138 72. Quezada, L.K. *et al.* Early transcriptional and epigenetic divergence of CD8+ T cells
1139 responding to acute versus chronic infection. *PLoS Biol* **21**, e3001983 (2023).
1140 73. Silva, J.G. *et al.* Emergence and fate of stem cell-like Tcf7(+) CD8(+) T cells during a
1141 primary immune response to viral infection. *Sci Immunol* **8**, eadh3113 (2023).
1142 74. Araki, K. *et al.* mTOR regulates memory CD8 T-cell differentiation. *Nature* **460**, 108-12
1143 (2009).
1144 75. Crowl, J.T. *et al.* Tissue-resident memory CD8(+) T cells possess unique transcriptional,
1145 epigenetic and functional adaptations to different tissue environments. *Nat Immunol* **23**,
1146 1121-1131 (2022).
1147 76. Renkema, K.R. *et al.* KLRG1(+) Memory CD8 T Cells Combine Properties of Short-Lived
1148 Effectors and Long-Lived Memory. *J Immunol* **205**, 1059-1069 (2020).
1149 77. Abboud, G. *et al.* Transcription Factor Bcl11b Controls Effector and Memory CD8 T cell
1150 Fate Decision and Function during Poxvirus Infection. *Front Immunol* **7**, 425 (2016).
1151 78. Helm, E.Y. *et al.* Bcl11b sustains multipotency and restricts effector programs of
1152 intestinal-resident memory CD8(+) T cells. *Sci Immunol* **8**, eabn0484 (2023).
1153 79. Connolly, K.A. *et al.* A reservoir of stem-like CD8(+) T cells in the tumor-draining lymph
1154 node preserves the ongoing antitumor immune response. *Sci Immunol* **6**, eabg7836
1155 (2021).
1156 80. Escobar, G. *et al.* Tumor immunogenicity dictates reliance on TCF1 in CD8(+) T cells for
1157 response to immunotherapy. *Cancer Cell* **41**, 1662-1679 e7 (2023).
1158 81. Mazet, J.M. *et al.* IFNgamma signaling in cytotoxic T cells restricts anti-tumor responses
1159 by inhibiting the maintenance and diversity of intra-tumoral stem-like T cells. *Nat*
1160 *Commun* **14**, 321 (2023).
1161 82. Tabilas, C., Smith, N.L. & Rudd, B.D. Shaping immunity for life: Layered development of
1162 CD8(+) T cells. *Immunol Rev* **315**, 108-125 (2023).
1163 83. Wang, J. *et al.* Fetal and adult progenitors give rise to unique populations of CD8+ T
1164 cells. *Blood* **128**, 3073-3082 (2016).
1165 84. Chopp, L.B. *et al.* An Integrated Epigenomic and Transcriptomic Map of Mouse and
1166 Human alphabeta T Cell Development. *Immunity* **53**, 1182-1201 e8 (2020).
1167 85. Steier, Z. *et al.* Single-cell multiomic analysis of thymocyte development reveals drivers
1168 of CD4(+) T cell and CD8(+) T cell lineage commitment. *Nat Immunol* **24**, 1579-1590
1169 (2023).
1170 86. Cyster, J.G. & Schwab, S.R. Sphingosine-1-phosphate and lymphocyte egress from
1171 lymphoid organs. *Annu Rev Immunol* **30**, 69-94 (2012).
1172 87. Hosokawa, H. *et al.* Bcl11b sets pro-T cell fate by site-specific cofactor recruitment and
1173 by repressing Id2 and Zbtb16. *Nat Immunol* **19**, 1427-1440 (2018).
1174 88. Mack, R., Zhang, L., Breslin Sj, P. & Zhang, J. The Fetal-to-Adult Hematopoietic Stem
1175 Cell Transition and its Role in Childhood Hematopoietic Malignancies. *Stem Cell Rev*
1176 *Rep* **17**, 2059-2080 (2021).
1177 89. Heo, I. *et al.* Lin28 mediates the terminal uridylation of let-7 precursor MicroRNA. *Mol*
1178 *Cell* **32**, 276-84 (2008).

1179 90. Yuan, J., Nguyen, C.K., Liu, X., Kanellopoulou, C. & Muljo, S.A. Lin28b reprograms adult
1180 bone marrow hematopoietic progenitors to mediate fetal-like lymphopoiesis. *Science*
1181 **335**, 1195-200 (2012).
1182 91. Wells, A.C. *et al.* Modulation of let-7 miRNAs controls the differentiation of effector CD8
1183 T cells. *Elife* **6**(2017).
1184 92. Horr, B. *et al.* Production and characterization of monoclonal antibodies to Xenopus
1185 proteins. *Development* **150**(2023).
1186 93. Hao, Y. *et al.* Integrated analysis of multimodal single-cell data. *Cell* **184**, 3573-3587 e29
1187 (2021).
1188 94. Contreras, A. *et al.* Co-transfer of tumor-specific effector and memory CD8+ T cells
1189 enhances the efficacy of adoptive melanoma immunotherapy in a mouse model. *J*
1190 *Immunother Cancer* **6**, 41 (2018).
1191 95. Love, M.I., Huber, W. & Anders, S. Moderated estimation of fold change and dispersion
1192 for RNA-seq data with DESeq2. *Genome Biol* **15**, 550 (2014).
1193 96. Zhou, Y. *et al.* Metascape provides a biologist-oriented resource for the analysis of
1194 systems-level datasets. *Nat Commun* **10**, 1523 (2019).
1195

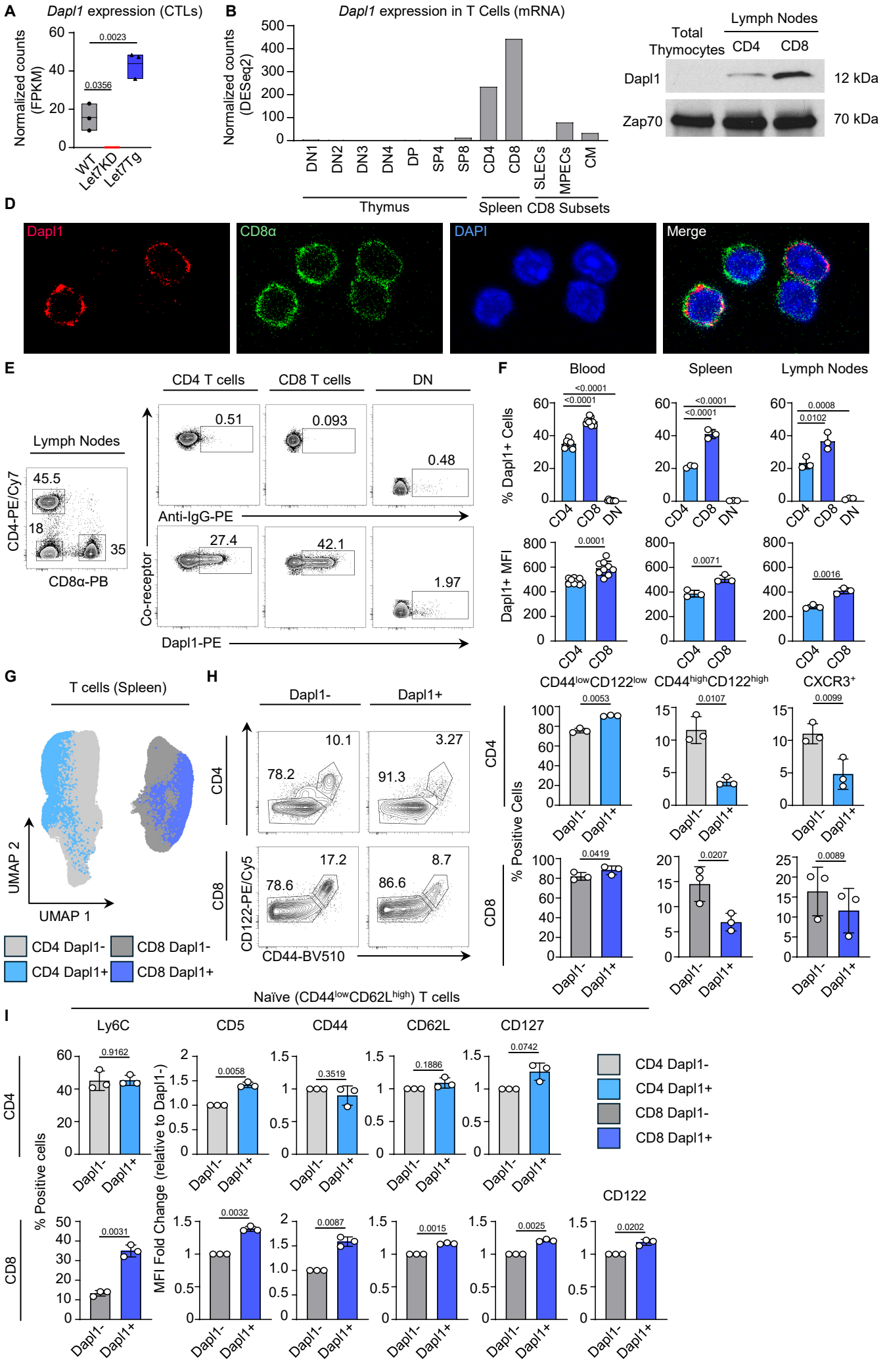
A
Dapl1 expression (CTLs)
Normalized counts (FPKM)
0.0023
0.0356
WT
Let7KD
Let7Tg
B
Dapl1 expression in T Cells (mRNA)
Normalized counts (DESeq2)
DN1
DN2
DN3
DN4
DP
SP4
SP8
CD4
CD8
SLECs
MPECs
CM
Thymus
Spleen
CD8 Subsets
Total Thymocytes
Lymph Nodes
CD4
CD8
Dapl1
Zap70
12 kDa
70 kDa
D
Dapl1
CD8α
DAPI
Merge
E
CD4 T cells
CD8 T cells
DN
Lymph Nodes
CD4-PE/Cy7
CD8α-PB
45.5
18
35
0.51
0.093
0.48
Anti-IgG-PE
27.4
42.1
1.97
Co-receptor
Dapl1-PE
F
Blood
Spleen
Lymph Nodes
% Dapl1+ Cells
<0.0001
<0.0001
<0.0001
<0.0001
0.0008
0.0102
CD4
CD8
DN
Dapl1+ MFI
0.0001
0.0071
0.0016
CD44lowCD122low
CD44highCD122high
CXCR3+
% Positive Cells
0.0053
0.0107
0.0099
0.0419
0.0207
0.0089
Dapl1-
Dapl1+
G
T cells (Spleen)
UMAP 2
UMAP 1
CD4 Dapl1-
CD8 Dapl1-
CD4 Dapl1+
CD8 Dapl1+
H
Dapl1-
Dapl1+
CD4
CD8
10.1
78.2
3.27
91.3
17.2
78.6
8.7
86.6
CD122-PE/Cy5
CD44-BV510
I
Naïve (CD44lowCD62Lhigh) T cells
Ly6C
CD5
CD44
CD62L
CD127
CD122
% Positive cells
MFI Fold Change (relative to Dapl1-)
0.9162
0.0058
0.3519
0.1886
0.0742
0.0031
0.0032
0.0087
0.0015
0.0025
0.0202
CD4 Dapl1-
CD4 Dapl1+
CD8 Dapl1-
CD8 Dapl1+

Figure 1

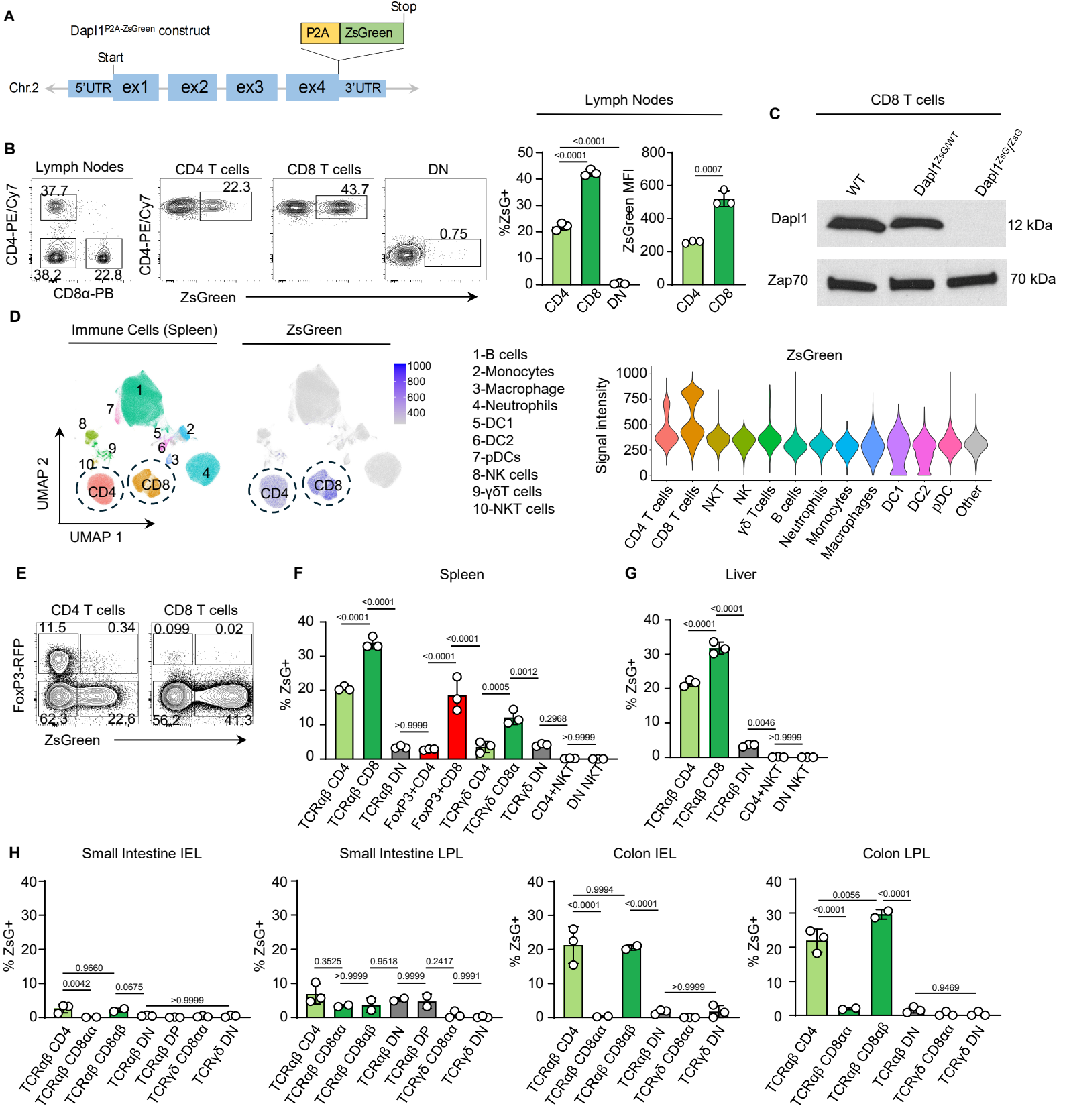
A
Dapl1P2A-ZsGreen construct
Stop
P2A
ZsGreen
Start
Chr.2
5'UTR
ex1
ex2
ex3
ex4
3'UTR
B
Lymph Nodes
CD4 T cells
CD8 T cells
DN
37.7
38.2
22.8
22.3
43.7
0.75
CD4-PE/Cy7
CD8α-PB
ZsGreen
Lymph Nodes
%ZsG+
ZsGreen MFI
<0.0001
0.0007
CD4
CD8
DN
C
CD8 T cells
WT
Dapl1ZsG/WT
Dapl1ZsG/ZsG
Dapl1
Zap70
12 kDa
70 kDa
D
Immune Cells (Spleen)
ZsGreen
UMAP 2
UMAP 1
CD4
CD8
1-B cells
2-Monocytes
3-Macrophage
4-Neutrophils
5-DC1
6-DC2
7-pDCs
8-NK cells
9-γδT cells
10-NKT cells
ZsGreen
Signal intensity
CD4 T cells
CD8 T cells
NKT
NK
γδ Tcells
B cells
Neutrophils
Monocytes
Macrophages
DC1
DC2
pDC
Other
E
CD4 T cells
CD8 T cells
11.5
0.34
62.3
22.6
0.099
0.02
56.2
41.3
FoxP3-RFP
ZsGreen
F
Spleen
% ZsG+
TCRαβ CD4
TCRαβ CD8
TCRαβ DN
FoxP3+CD4
FoxP3+CD8
TCRγδ CD4
TCRγδ CD8α
TCRγδ DN
CD4+NKT
DN NKT
G
Liver
H
Small Intestine IEL
Small Intestine LPL
Colon IEL
Colon LPL
TCRαβ CD8αα
TCRαβ CD8αβ
TCRαβ DP
TCRγδ CD8αα

Figure 2

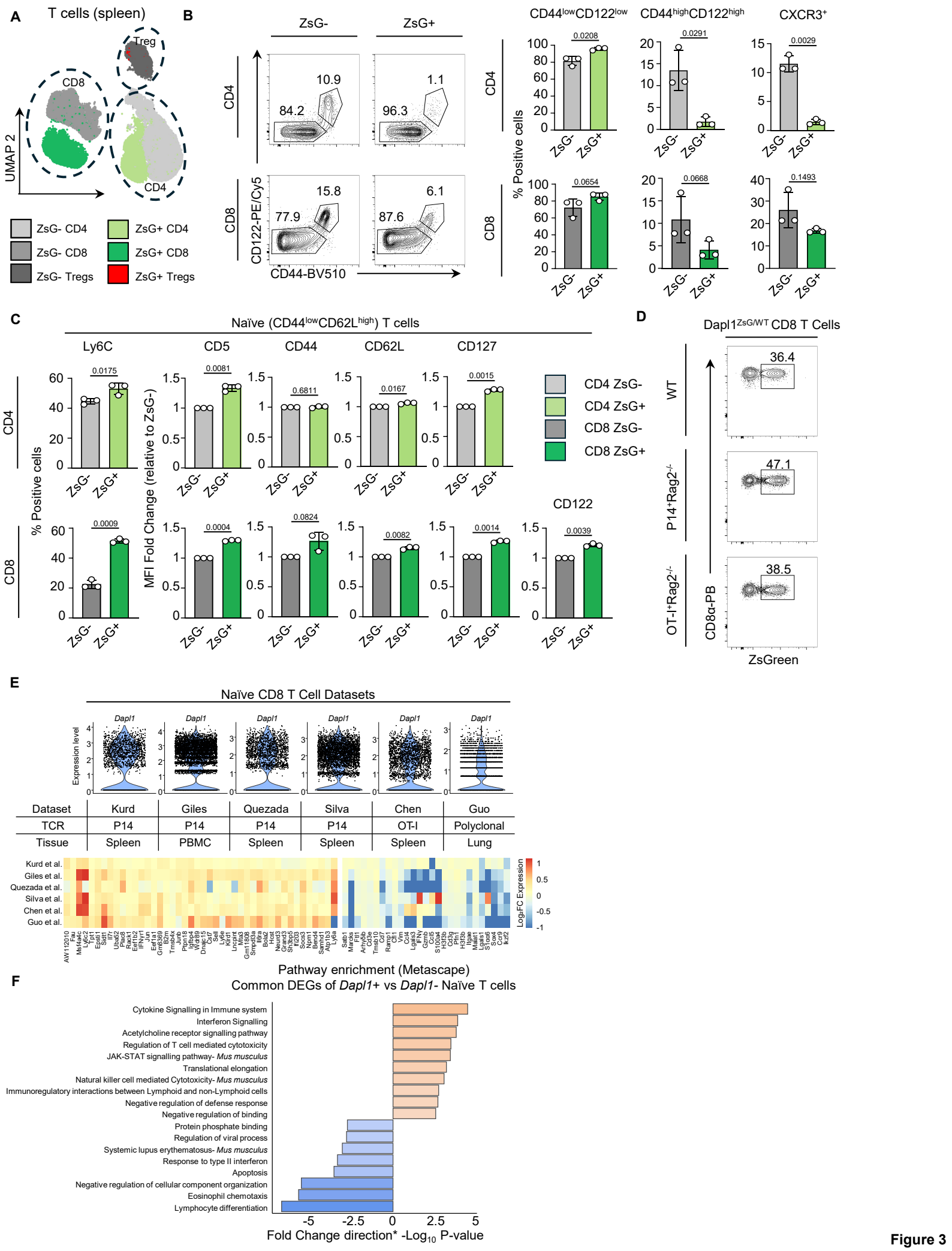
A
T cells (spleen)
Treg
CD8
CD4
UMAP 2
ZsG- CD4
ZsG- CD8
ZsG- Tregs
ZsG+ CD4
ZsG+ CD8
ZsG+ Tregs
B
ZsG-
ZsG+
CD4
CD8
10.9
84.2
1.1
96.3
15.8
77.9
6.1
87.6
CD122-PE/Cy5
CD44-BV510
CD44lowCD122low
CD44highCD122high
CXCR3+
% Positive cells
0.0208
0.0291
0.0029
0.0654
0.0668
0.1493
C
Naïve (CD44lowCD62Lhigh) T cells
Ly6C
CD5
CD44
CD62L
CD127
CD122
MFI Fold Change (relative to ZsG-)
0.0175
0.0081
0.6811
0.0167
0.0015
0.0009
0.0004
0.0824
0.0082
0.0014
0.0039
CD4 ZsG-
CD4 ZsG+
CD8 ZsG-
CD8 ZsG+
D
Dapl1ZsG/WT CD8 T Cells
WT
P14+Rag2-/-
OT-I+Rag2-/-
36.4
47.1
38.5
CD8α-PB
ZsGreen
E
Naïve CD8 T Cell Datasets
Dapl1
Expression level
Dataset
Kurd
Giles
Quezada
Silva
Chen
Guo
TCR
P14
P14
P14
P14
OT-I
Polyclonal
Tissue
Spleen
PBMC
Spleen
Spleen
Spleen
Lung
Kurd et al.
Giles et al.
Quezada et al.
Silva et al.
Chen et al.
Guo et al.
LogFC Expression
Pathway enrichment (Metascape)
F
Common DEGs of Dapl1+ vs Dapl1- Naïve T cells
Cytokine Signalling in Immune system
Interferon Signalling
Acetylcholine receptor signalling pathway
Regulation of T cell mediated cytotoxicity
JAK-STAT signalling pathway- Mus musculus
Translational elongation
Natural killer cell mediated Cytotoxicity- Mus musculus
Immunoregulatory interactions between Lymphoid and non-Lymphoid cells
Negative regulation of defense response
Negative regulation of binding
Protein phosphate binding
Regulation of viral process
Systemic lupus erythematosus- Mus musculus
Response to type II interferon
Apoptosis
Negative regulation of cellular component organization
Eosinophil chemotaxis
Lymphocyte differentiation
Fold Change direction* -Log10 P-value

Figure 3

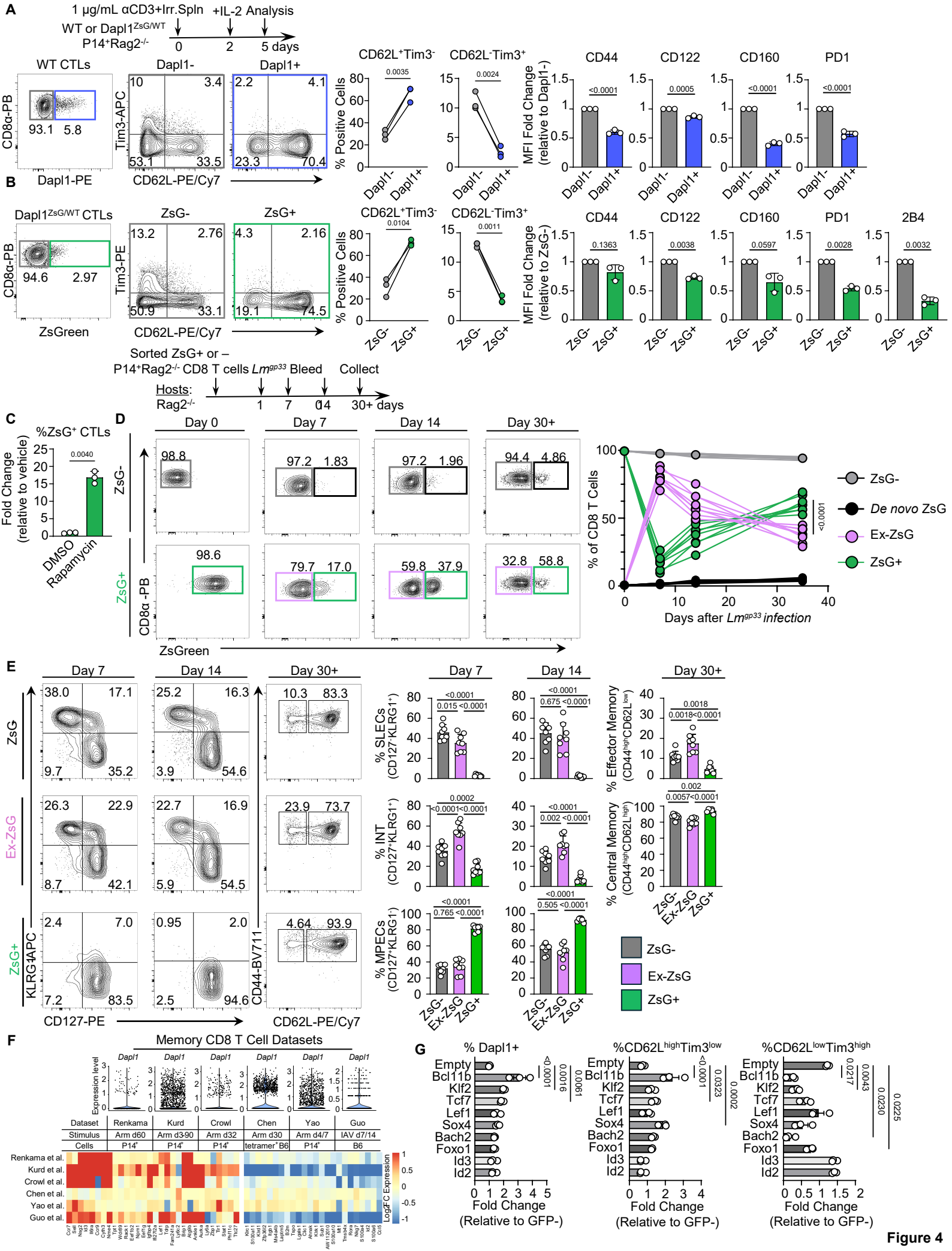
A
1 µg/mL αCD3+Irr.Spln +IL-2 Analysis
WT or Dapl1ZsG/WT
P14+Rag2-/-
0 2 5 days
WT CTLs
Dapl1-
Dapl1+
CD8α-PB
Dapl1-PE
Tim3-APC
CD62L-PE/Cy7
93.1 5.8
10 3.4
53.1 33.5
2.2 4.1
23.3 70.4
CD62L+Tim3-
CD62L-Tim3+
% Positive Cells
0.0035
0.0024
MFI Fold Change (relative to Dapl1-)
CD44
CD122
CD160
PD1
<0.0001
0.0005
<0.0001
<0.0001
B
Dapl1ZsG/WT CTLs
ZsG-
ZsG+
CD8α-PB
ZsGreen
Tim3-PE
CD62L-PE/Cy7
94.6 2.97
13.2 2.76
50.9 33.1
4.3 2.16
19.1 74.5
0.0104
0.0011
MFI Fold Change (relative to ZsG-)
2B4
0.1363
0.0038
0.0597
0.0028
0.0032
Sorted ZsG+ or – P14+Rag2-/- CD8 T cells Lmgp33 Bleed Collect
Hosts: Rag2-/-
1 7 14 30+ days
C
%ZsG+ CTLs
Fold Change (relative to vehicle)
0.0040
DMSO
Rapamycin
D
Day 0
Day 7
Day 14
Day 30+
98.8
97.2 1.83
97.2 1.96
94.4 4.86
98.6
79.7 17.0
59.8 37.9
32.8 58.8
% of CD8 T Cells
Days after Lmgp33 infection
<0.0001
ZsG-
De novo ZsG
Ex-ZsG
ZsG+
E
Day 7
Day 14
Day 30+
38.0 17.1
9.7 35.2
25.2 16.3
3.9 54.6
10.3 83.3
26.3 22.9
8.7 42.1
22.7 16.9
5.9 54.5
23.9 73.7
2.4 7.0
7.2 83.5
0.95 2.0
2.5 94.6
4.64 93.9
KLRG1APC
CD127-PE
CD44-BV711
CD62L-PE/Cy7
% SLECs (CD127+KLRG1+)
% INT (CD127+KLRG1-)
% MPECs (CD127+KLRG1-)
% Effector Memory (CD44highCD62Llow)
% Central Memory (CD44highCD62Lhigh)
<0.0001
0.015 <0.0001
0.675 <0.0001
0.0018
0.0018<0.0001
0.0002
<0.0001<0.0001
0.002 <0.0001
0.002
0.0057<0.0001
0.765 <0.0001
0.505 <0.0001
ZsG-
Ex-ZsG
ZsG+
F
Memory CD8 T Cell Datasets
Dapl1
Expression level
Dataset
Renkama
Kurd
Crowl
Chen
Yao
Guo
Stimulus
Arm d60
Arm d3-90
Arm d32
Arm d30
Arm d4/7
IAV d7/14
Cells
P14+
tetramer+B6
B6
Renkama et al.
Kurd et al.
Crowl et al.
Chen et al.
Yao et al.
Guo et al.
LogFC Expression
G
% Dapl1+
%CD62LhighTim3low
%CD62LlowTim3high
Empty
Bcl11b
Klf2
Tcf7
Lef1
Sox4
Bach2
Foxo1
Id3
Id2
<0.0001
0.0016
0.0061
0.0323
0.0002
0.0217
0.0043
0.0230
0.0225
Fold Change (Relative to GFP-)

Figure 4

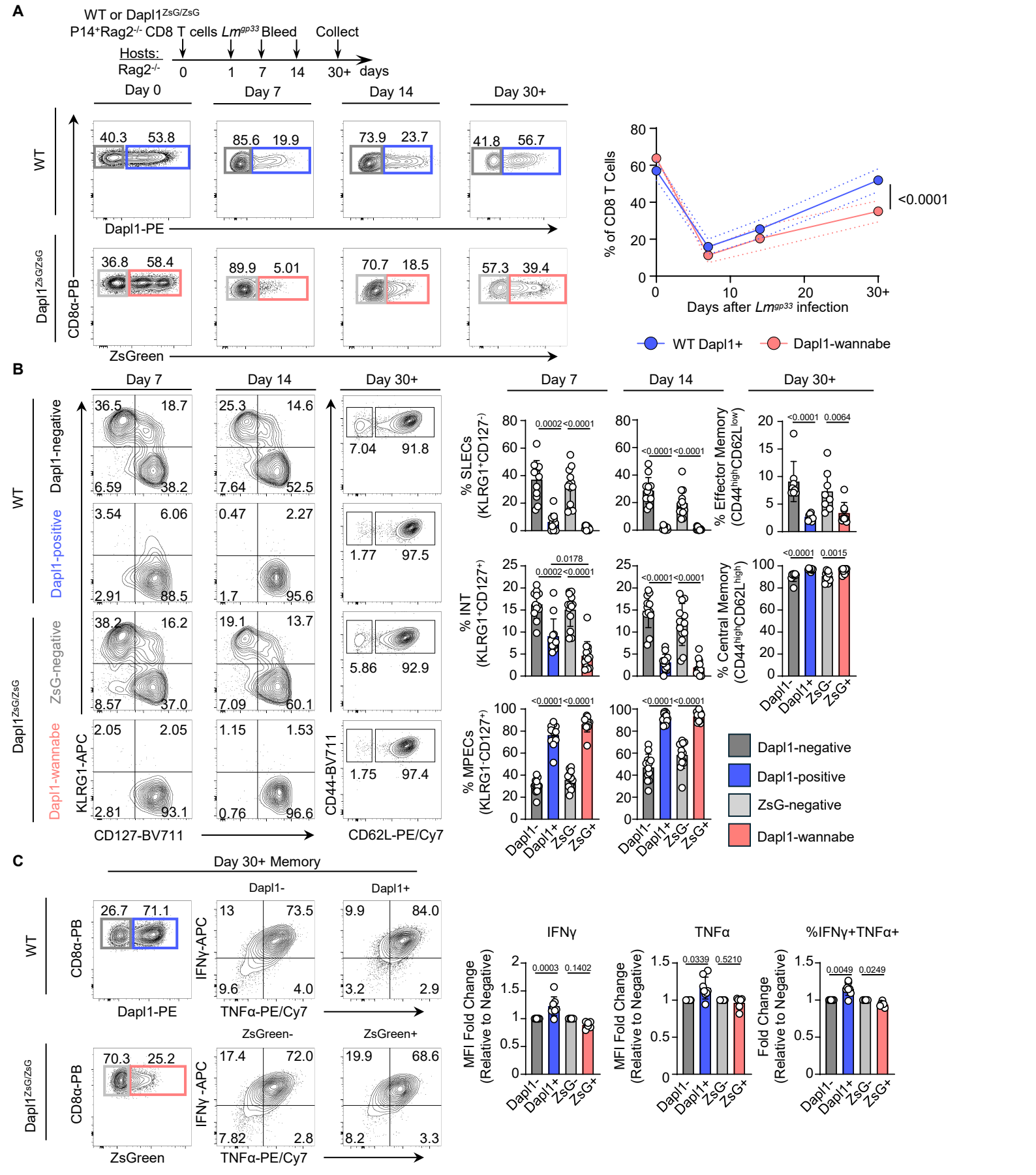
A
WT or Dapl1ZsG/ZsG
P14+Rag2-/- CD8 T cells Lmgp33 Bleed
Collect
Hosts: Rag2-/-
0 1 7 14 30+ days
Day 0
Day 7
Day 14
Day 30+
WT
Dapl1ZsG/ZsG
CD8α-PB
Dapl1-PE
ZsGreen
40.3 53.8
85.6 19.9
73.9 23.7
41.8 56.7
36.8 58.4
89.9 5.01
70.7 18.5
57.3 39.4
% of CD8 T Cells
Days after Lmgp33 infection
<0.0001
WT Dapl1+
Dapl1-wannabe
B
Dapl1-negative
Dapl1-positive
ZsG-negative
Dapl1-wannabe
KLRG1-APC
CD127-BV711
CD44-BV711
CD62L-PE/Cy7
36.5 18.7 6.59 38.2
25.3 14.6 7.64 52.5
7.04 91.8
3.54 6.06 2.91 88.5
0.47 2.27 1.7 95.6
1.77 97.5
38.2 16.2 8.57 37.0
19.1 13.7 7.09 60.1
5.86 92.9
2.05 2.05 2.81 93.1
1.15 1.53 0.76 96.6
1.75 97.4
% SLECs (KLRG1+CD127-)
% INT (KLRG1+CD127+)
% MPECs (KLRG1-CD127+)
% Effector Memory (CD44highCD62Llow)
% Central Memory (CD44highCD62Lhigh)
Dapl1-negative
Dapl1-positive
ZsG-negative
Dapl1-wannabe
C
Day 30+ Memory
Dapl1-
Dapl1+
ZsGreen-
ZsGreen+
IFNγ-APC
TNFα-PE/Cy7
26.7 71.1
13 73.5 9.6 4.0
9.9 84.0 3.2 2.9
70.3 25.2
17.4 72.0 7.82 2.8
19.9 68.6 8.2 3.3
IFNγ
TNFα
%IFNγ+TNFα+
MFI Fold Change (Relative to Negative)
Fold Change (Relative to Negative)

Figure 5

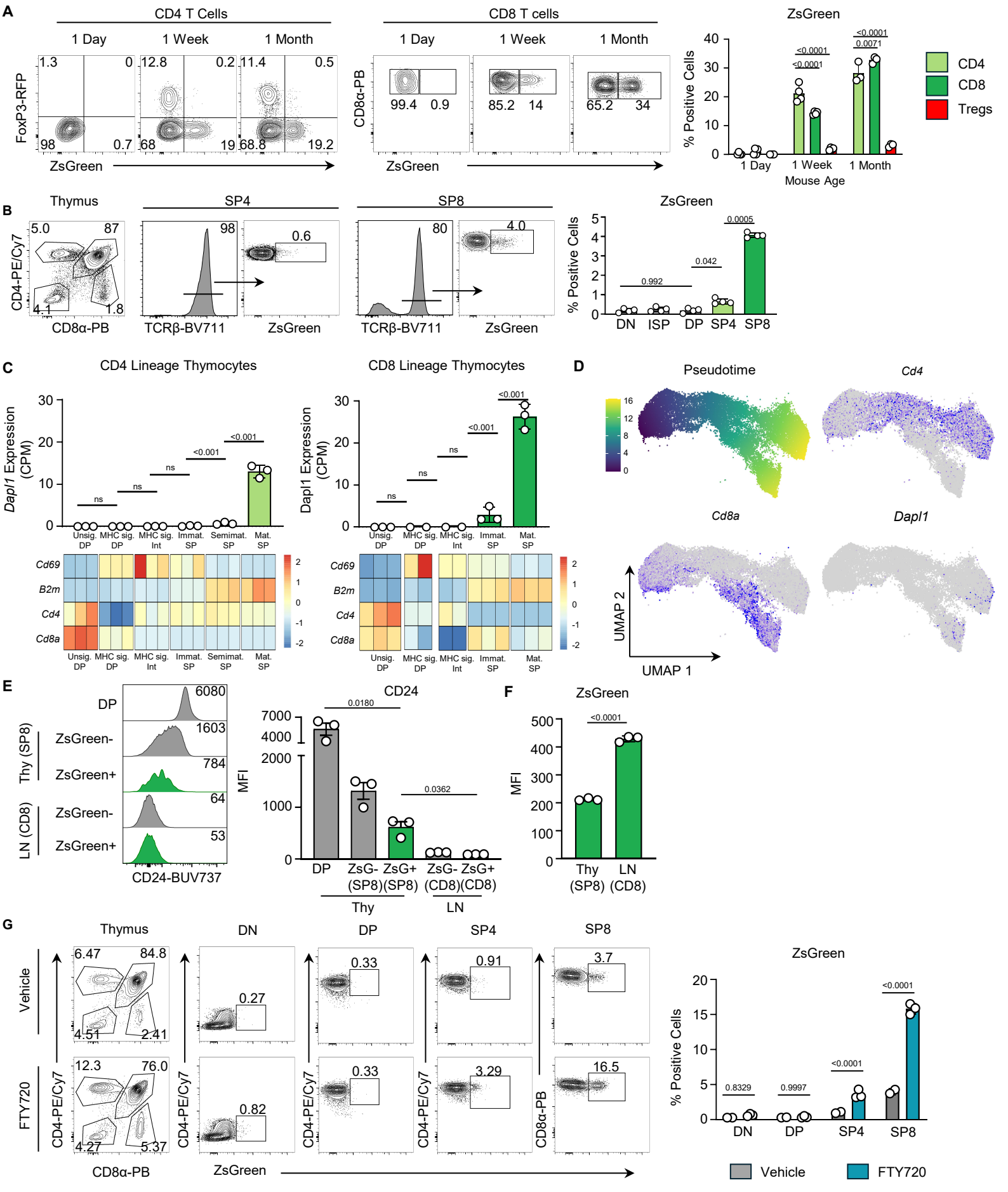
A
CD4 T Cells
1 Day
1 Week
1 Month
FoxP3-RFP
ZsGreen
1.3
0
98
0.7
12.8
0.2
68
19
11.4
0.5
68.8
19.2
CD8 T cells
CD8α-PB
99.4
0.9
85.2
14
65.2
34
ZsGreen
% Positive Cells
<0.0001
<0.0001
<0.0001
0.0071
CD4
CD8
Tregs
Mouse Age
B
Thymus
SP4
SP8
CD4-PE/Cy7
CD8α-PB
TCRβ-BV711
5.0
87
4.1
1.8
98
0.6
80
4.0
0.992
0.042
0.0005
DN
ISP
DP
SP4
SP8
C
CD4 Lineage Thymocytes
CD8 Lineage Thymocytes
Dapl1 Expression (CPM)
ns
<0.001
Unsig. DP
MHC sig. DP
MHC sig. Int
Immat. SP
Semimat. SP
Mat. SP
Cd69
B2m
Cd4
Cd8a
D
Pseudotime
Cd4
Cd8a
Dapl1
UMAP 2
UMAP 1
E
DP
ZsGreen-
ZsGreen+
Thy (SP8)
LN (CD8)
6080
1603
784
64
53
CD24-BUV737
CD24
MFI
0.0180
0.0362
ZsG- (SP8)
ZsG+ (SP8)
ZsG- (CD8)
ZsG+ (CD8)
Thy
LN
F
ZsGreen
<0.0001
Thy (SP8)
LN (CD8)
G
Thymus
DN
DP
SP4
SP8
Vehicle
FTY720
6.47
84.8
4.51
2.41
12.3
76.0
4.27
5.37
0.27
0.82
0.33
0.33
0.91
3.29
3.7
16.5
CD4-PE/Cy7
CD8α-PB
ZsGreen
% Positive Cells
0.8329
0.9997
<0.0001
<0.0001
Vehicle
FTY720

Figure 6

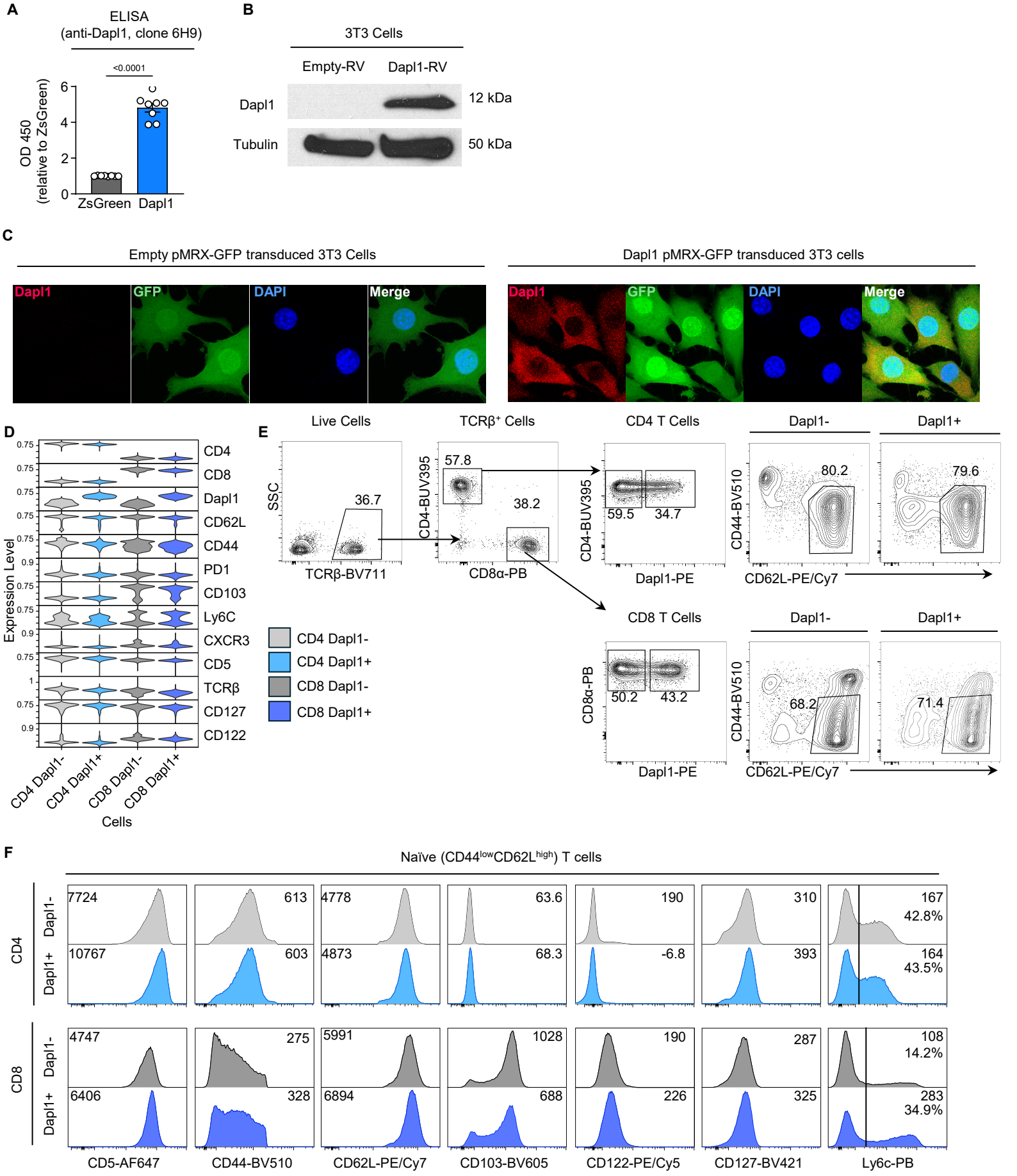

Supplementary Figure 1

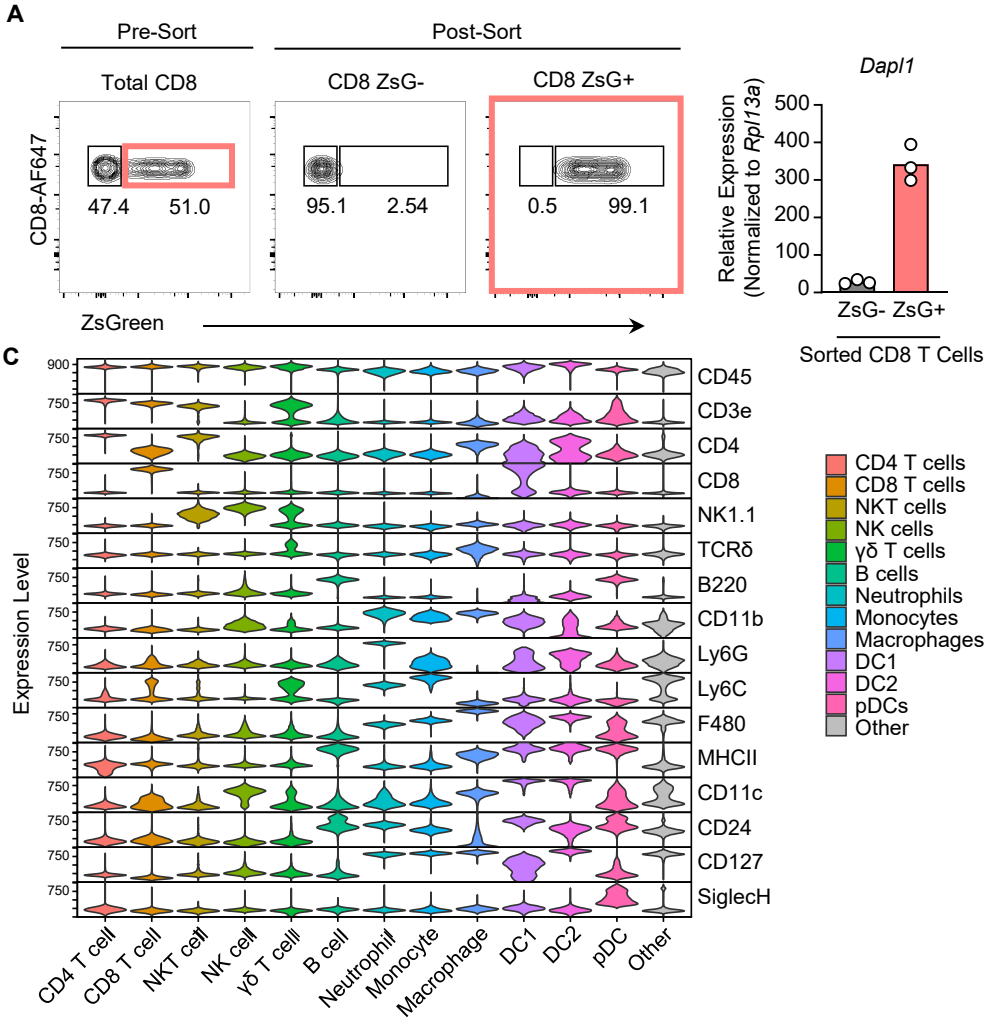

Supplementary Figure 2

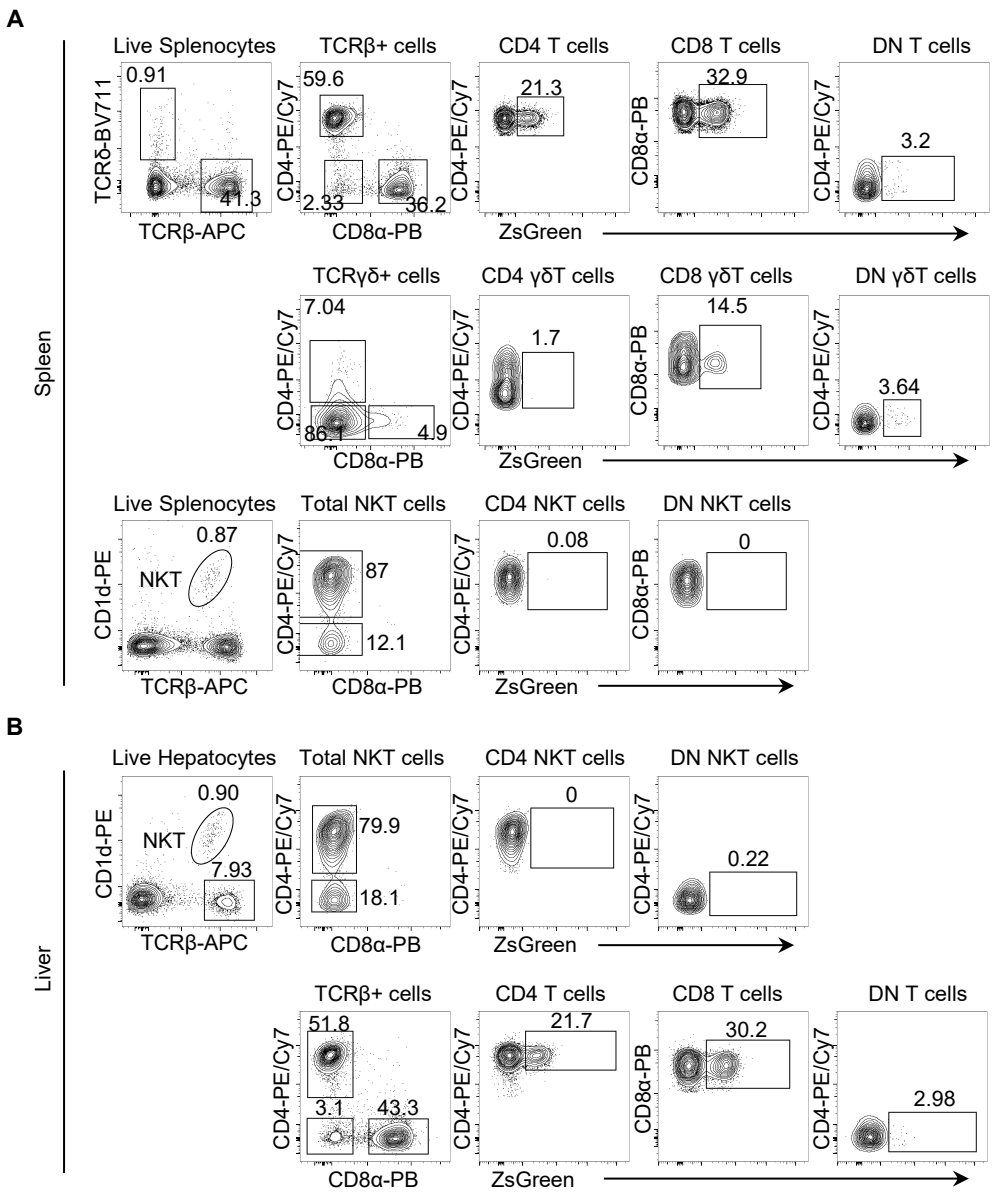

Supplementary Figure 3

Supplementary Figure 4

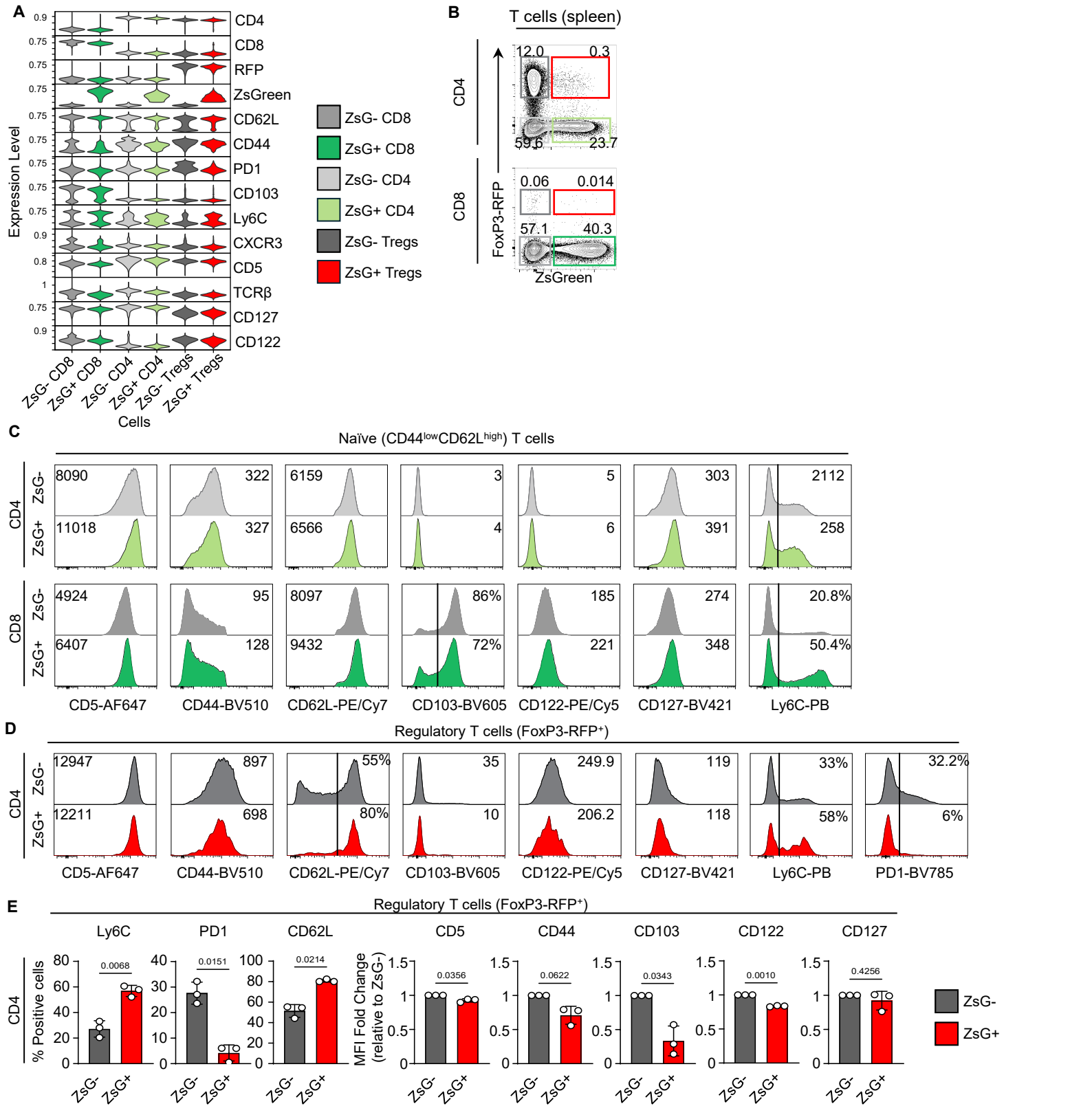

Supplementary Figure 5

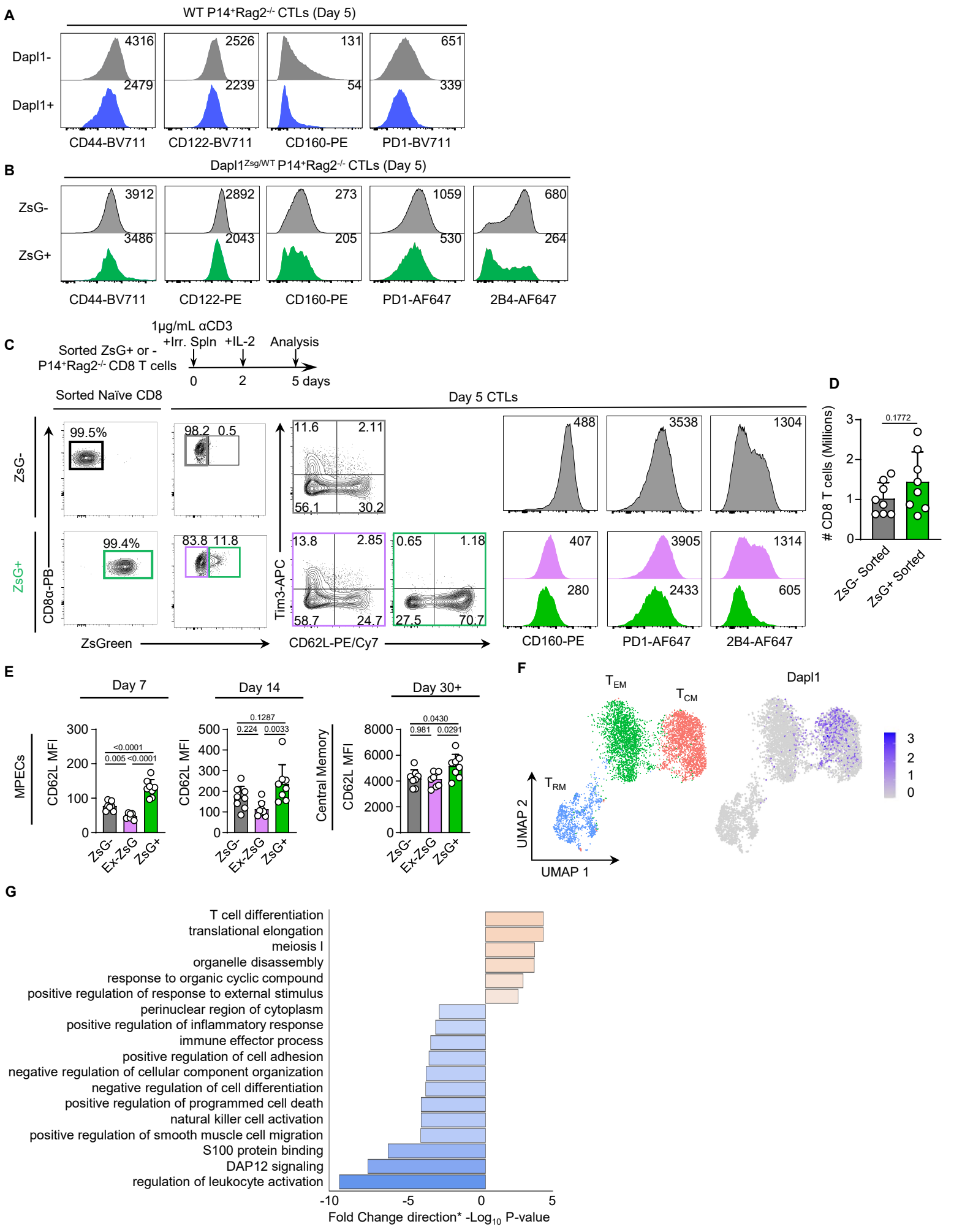

Supplementary figure 6

A

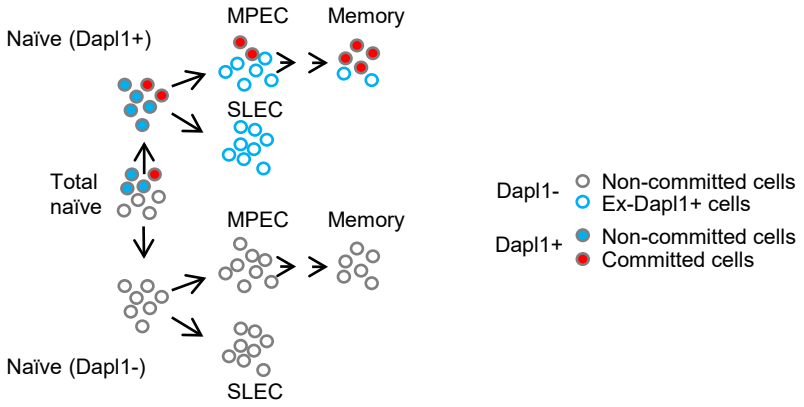

Supplementary figure 7

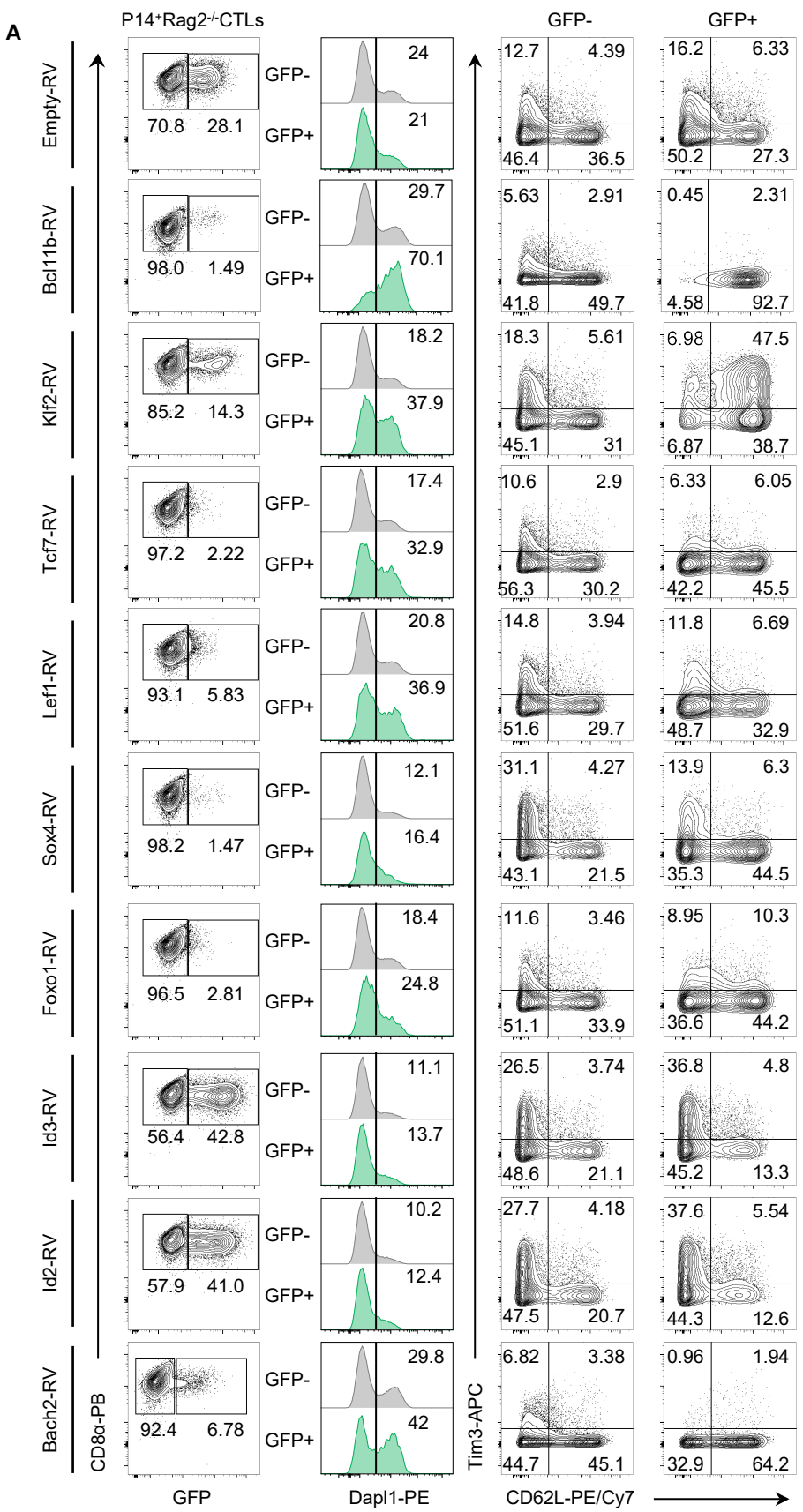

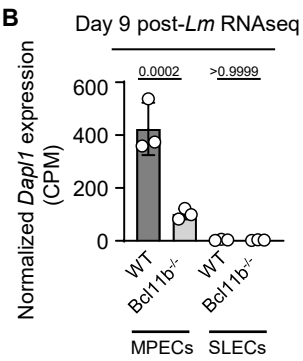

Supplementary figure 8

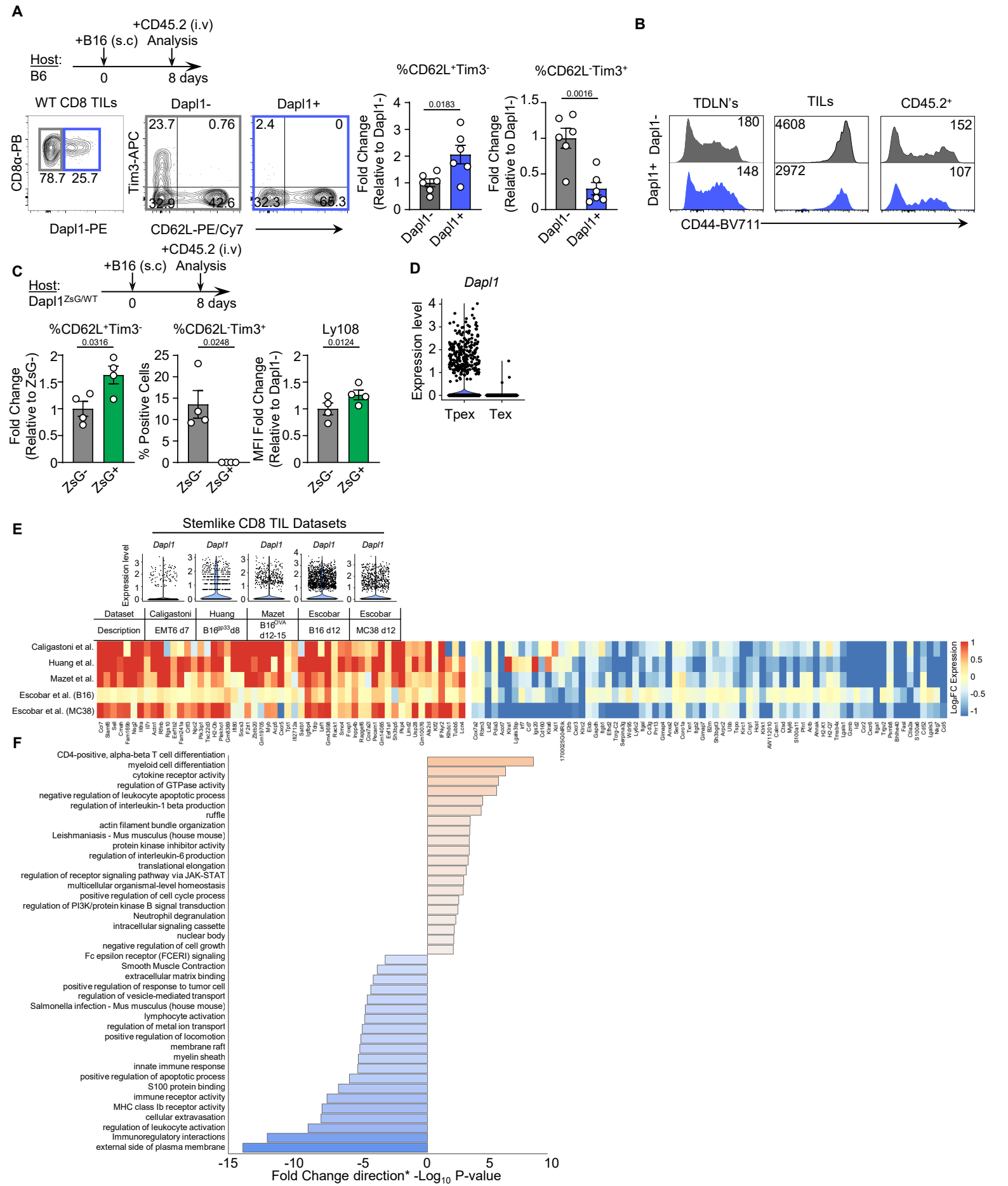

Supplementary figure 9

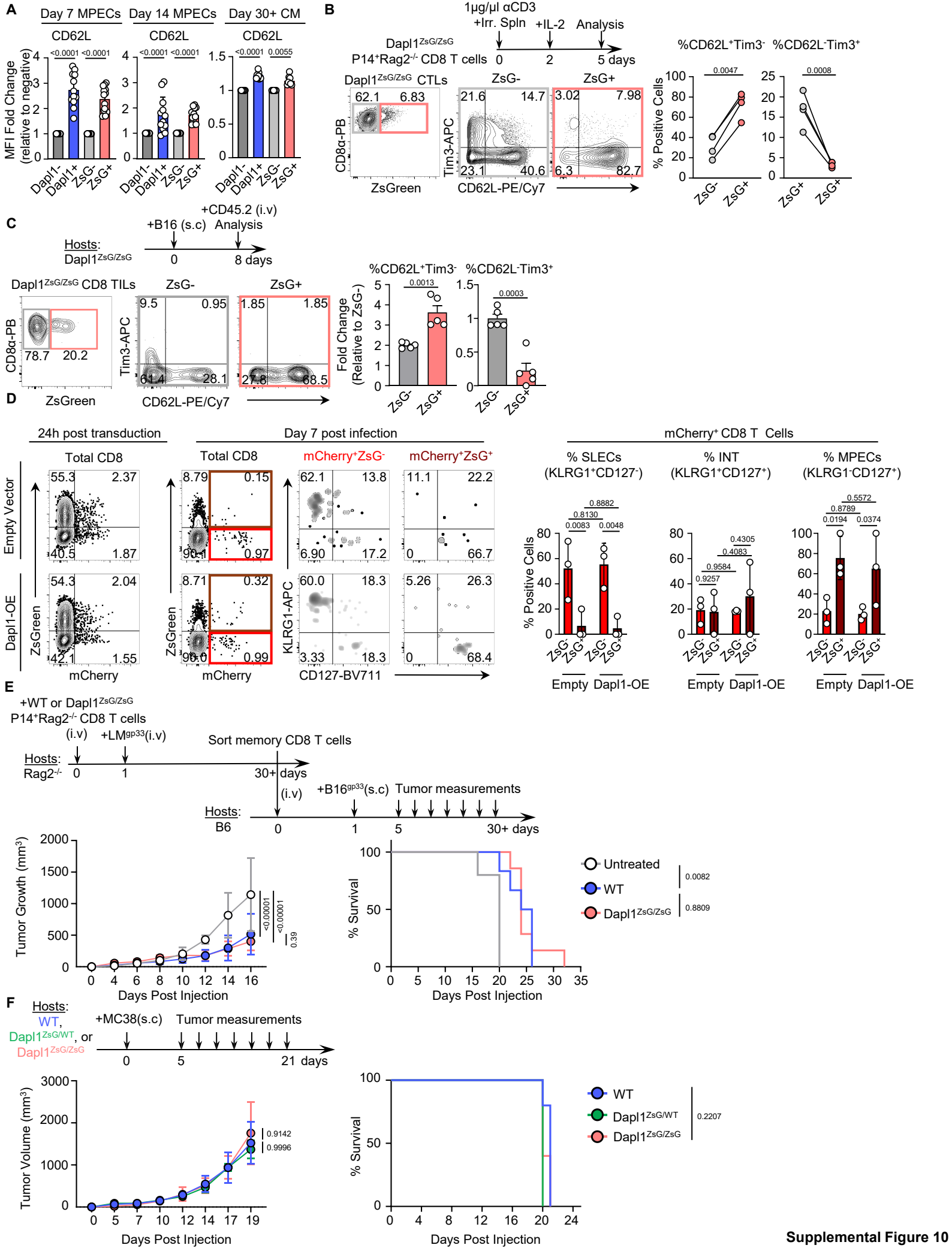

Supplemental Figure 10

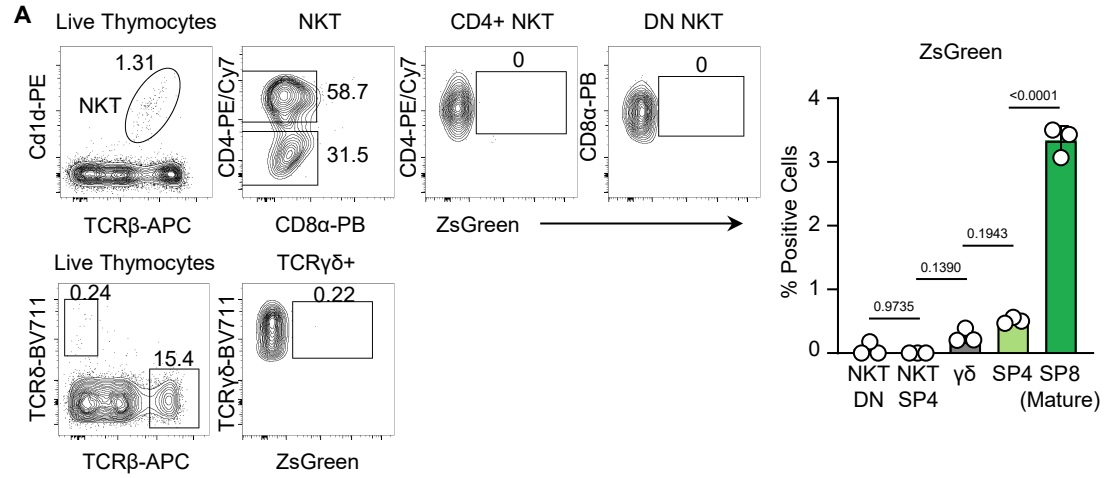

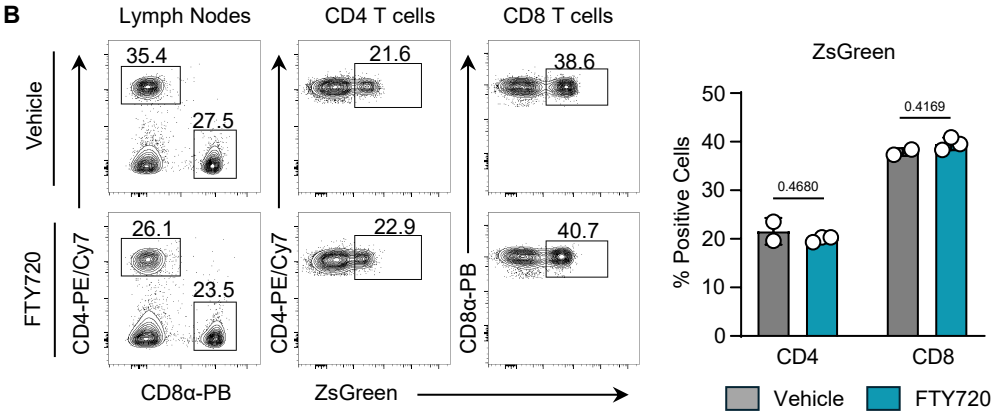

Supplementary Figure 11